Alma Mater Studiorum · University of Bologna

School of Science
Department of Physics and Astronomy
Bachelor Degree in Physics

Reconstruction of Λ_c^+ signal in ALICE experiment using neural networks with TMVA

Supervisor:
Prof. Andrea Alici

Submitted by:
Camilla Berti

Academic Year 2023/2024

Ai miei nonni e alla tata Anna,
la prima cosa bella
che ho avuto dalla vita.

Abstract

Circa 10^{-6} secondi dopo il Big Bang, l'universo si è trovato in condizioni di temperatura e densità di energia estremamente elevate, in uno stato deconfinato di quark e gluoni noto come plasma di quark e gluoni. Questo stato può essere ricreato al Large Hadron Collider attraverso collisioni di ioni pesanti, il cui studio rappresenta uno dei principali obiettivi dell'esperimento ALICE.
I quark charm and beauty sono ideali per studiare il plasma di quark e gluoni, perché, a causa della loro elevata massa, vengono prodotti all'inizio della collisione e rimangono presenti durante tutta l'evoluzione del sistema. Inoltre, misurare la produzione degli adroni charmati, consente anche di investigare i rapporti fra i vari adroni che vengono prodotti in funzione del momento trasverso, utili nella comprensione dei meccanismi di adronizzazione dei quark charm. In particolare, misure di ALICE in collisioni pp hanno mostrato un aumento nella produzione di barioni charmati rispetto alle previsioni teoriche basate sull'universalità del processo di frammentazione. Nuovi modelli sono stati proposti per spiegare i risultati di ALICE, che riproducono generalmente l'andamento dei dati, ma differiscono nella regione di basso impulso trasverso. Risulta quindi fondamentale ottenere misure sperimentali precise proprio in questa regione, per discriminare fra i modelli proposti.
In questo lavoro di tesi è stato ricostruito il segnale del barione charmato Λ_c^+ a partire dai dati sperimentali raccolti da ALICE con collisioni pp a $\sqrt{s} = 13\,\text{TeV}$ nell'intervallo di impulso trasverso $1 < p_T < 2\,\text{GeV/c}$. A causa dell'elevato fondo combinatoriale e della breve vita media del barione Λ_c^+ è stato necessario l'uso di reti neurali implementate in TMVA per ricostruire il segnale. Diverse versioni dell'algoritmo sono state implementate e testate, permettendo di ricavare lo *yield*, cioè il numero effettivo di barioni Λ_c^+ ricostruiti.

Contents

Introduction

Understanding nature is one of the main goals of science. In the reductionist approach, one tries to explain all manifestations of reality using a compact set of relations. Such an approach has proved to be successful in pinning down fundamental interactions, and discovering the basic building blocks of the universe. We have found that the physical principles become simpler and simpler, not in the sense that the mathematics gets easier or that we always find fewer particles in the list of the elementary ones, but rather the fact that the discovered rules become increasingly coherent and universal. This provides an important insight, as the simplicity and beauty which are found in the fundamental laws mirrors something that is deeply built into the logical structure of the universe.
Our knowledge on fundamental physics is encoded in the Standard Model (SM), a framework of particle physics that describes the electromagnetic, weak and strong interactions. Quantum Chromodynamics (QCD) in particular describe the strong interaction. To get a comprehensive understanding of QCD is important to study extended systems subject to the strong force, that present features that do not directly arise from the laws governing microscopic interactions. As a parallel, in condensed matter physics, phenomena like magnetism and superconductivity improved the comprehension of the electromagnetic interaction. A system like this for QCD is the quark-gluon plasma, a state of matter in which quarks and gluons are bounded only weakly and are free to move. Quark-gluon plasma is also fascinating because it is believed that the universe was in such state about 10^{-6} s after the Big Bang. Nowadays, it is replicated at the Large Hadron Collider (LHC) with heavy-ions collisions at CERN, in Geneva. The ALICE experiment is optimized to study these collisions: recreating this primordial state of matter and understanding its evolution will allow us to clarify questions about how matter is organized and the mechanism that confine quarks and gluons. The ALICE Collaboration carries out a comprehensive study of the particles produced by heavy-ions, proton-nucleus and proton-proton collisions, both as a comparison with nucleus-nucleus collisions and in their own right.
Specifically, measurements of the production cross sections of heavy-flavor (charm and beauty) hadrons are interesting because they are created at the very initial stage of a collision, so they experience the whole evolution of quark-gluon plasma and can provide important information for this research area. Recent analysis of ALICE data have shown

that, with respect to e^+e^- and ep collisions, there is an unexpected enhancement of the baryon production in pp collisions, that serves as a basis to comprehend the higher multiplicity heavy-ions collisions. New theoretical models have been created to explain this result and in order to discriminate between them it is essential to get precise values of baryon production. Doing this for the Λ_c^+ baryon, whose quark content is udc, is not trivial, especially at low transverse momentum. The Λ_c^+ baryon has a short mean life: $c\tau \approx 60\,\mu\text{m}$, so after it is created in the interaction point of the collision, it decays after it has travelled a small stretch. The small displacement of the decay vertex of Λ_c^+ from the interaction vertex is below the detector resolution, making a topological selection inadequate. Moreover, there is a high percentage of background, so these two issues make the use of alternative reconstruction and selection techniques to extract a significant signal necessary. In this thesis, the signal of Λ_c^+ was reconstructed using machine learning techniques, in particular with neural networks, used within TMVA, a toolkit integrated in ROOT.
The thesis is structured in the following chapters: in chapter 1, the theoretical background is presented together with the experimental results that motivated the analysis. Chapter 2 consists in a description of ALICE and its detectors that provided data for this work. In chapter 3 an overview of neural networks is outlined, while in chapter 4 the analysis is described and the output plots are shown. Finally, in the conclusions the achieved results are summarized.

Chapter 1

QGP and hadronisation of heavy flavor quarks

1.1 The Standard Model

According to our current understanding, the matter around us interacts through four fundamental forces: gravitational, weak, electromagnetic and strong interactions. The elementary blocks of matter are fermions, particles with half-integer spin, and their interactions are mediated through the exchange of force carriers, gauge bosons, which have integer spin. The Standard Model (SM) provides a framework for modern particle physics, describing elementary particles and three of the fundamental interactions that govern them. In the SM there are twelve fermions and five bosons; a schematic representation is depicted in figure 1.1. Each boson is associated with a specific interaction: the photon mediates the electromagnetic one, the strong nuclear force is carried by the gluons, and the weak nuclear one by the W and Z bosons. Each interaction has an associated charge that particles must have in order to participate: electric charge for the electromagnetic force, color charge for the strong force, and weak charge for the weak one.
Fermions are the particles that make up matter. They are categorized into three generations. Each generation contains two leptons and two quarks, with the main difference being that quarks have a color charge, whereas leptons do not. The lightest and most stable particles make up the first generation, whereas the heavier and less-stable particles belong to the second and third generations. Quarks come in six flavors: *up, down, strange, charm, beauty*, and *top*.
The Higgs field and the spontaneous symmetry breaking was introduced with the so-called Brout-Englert-Higgs mechanism to explain the fact that the weak force carriers, the W and Z bosons, are massive. Later it turned out that the other elementary particles also acquire masses by interacting with the Higgs boson: the stronger a particle

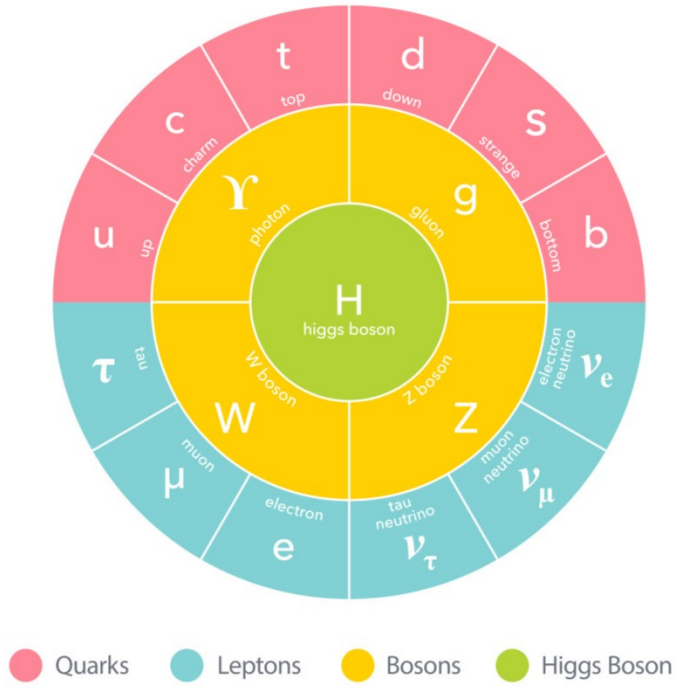

Figure 1.1: Fundamental particles of the Standard Model of particle physics.

interacts with the Higgs field, the heavier the particle ends up being. The Higgs boson is the only known elementary particle with spin 0 [1]. For each of these particles, there exists a corresponding antiparticle with opposite charges (some particles are their own antiparticle, such as the photon).
The Standard Model has successfully explained most experimental results and precisely predicted a wide range of phenomena. The Large Hadron Collider (LHC), the world's largest and most powerful particle accelerator, has played a crucial role in confirming the predictions of the SM. For instance, the predicted existence of the Higgs boson was confirmed by the observations made in 2012 by the ATLAS and CMS detectors at the LHC. However, there are also important questions that so far are not addressed by this theory, like dark matter, the asymmetry between matter and antimatter, the great difference in mass among the three generations and gravity. In fact, gravitational interaction is described by the general theory of relativity, but it is not included in the Standard Model. Ongoing experiments at the LHC provide valuable insights to answer these questions and in further testing the Standard Model [2, 3].

1.2 Quantum Chromodynamics

The strong interaction between quarks and gluons is formulated as a non-abelian gauge field theory called Quantum Chromodynamics (QCD) based on the invariance under $SU(3)_c$ group transformations.
In QCD, color plays the role of electric charge in QED and the force between quarks is mediated by the exchange of eight massless gluons of spin 1. Unlike electrodynamics, where there is only one kind of electric charge, there are three kinds of charges, conventionally referred to as color charges: red, green and blue. In the fundamental vertex q $\rightarrow$ q+ g the color of the quark may change. Since color is always conserved, this means that the gluon must carry away the difference, in fact each gluon carries a color and an anticolor charge. Since gluons themselves carry color (unlike the photon, which is electrically neutral), they couple directly to other gluons, and hence in addition to the fundamental quark-gluon vertex, we also have primitive gluon-gluon vertices. To represent more complicated process two or more fundamental vertices, illustrated in figure 1.2, are combined. The direct gluon-gluon coupling makes chromodynamics a lot more

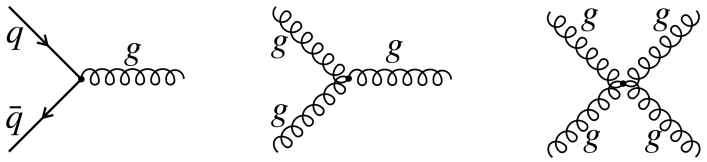

Figure 1.2: Feynman diagrams for the quark–gluon vertex (left), three-gluon interaction (middle) and four-gluon interaction (right).

complicated than electrodynamics but also far richer, with the possibility of hadronic states formed only by gluons, the so-called glueballs.

The strong coupling constant α_S for the strong force depends on the momentum transfer Q^2 (that's why it is called *running* coupling constant). It can be described as follows:

$$\alpha_S(Q^2) = \frac{16\pi^2}{(11 - \frac{2}{3}N_f)\ln Q^2/\Lambda^2_{\mathrm{QCD}}} \tag{1.1}$$

where Λ_{QCD} is the scale parameter and N_f is the number of light quarks. Experimental results of α_S measurements are showed in figure 1.3. At high energy the coupling is sufficiently weak so that it can be treated with a perturbative approach, already tested in QED. This phenomenon in which the interaction weakens as the distance decreases (large Q^2), is known as *asymptotic freedom*. Instead at large distances, when $\alpha_S \gtrsim 1$ the perturbative QCD (pQCD) is doomed because it turns out that the more complex Feynman diagrams should contribute more and more.

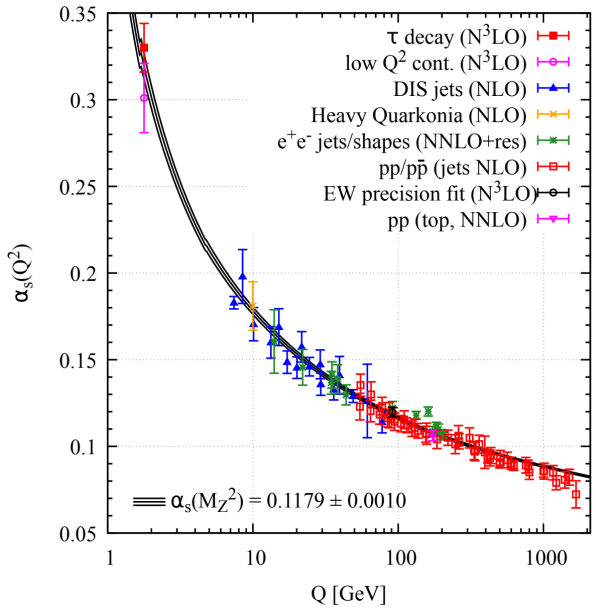

Figure 1.3: Summary of measurements of α_S as a function of the energy scale Q. The respective degree of QCD perturbation theory used in the extraction of α_S is indicated in brackets. Figure taken from [4].

Another important characteristic of QCD is that no naturally occurring particles carry color. Quarks are confined in colorless packages of a pair of quark and antiquark (mesons) or three quarks or antiquarks (baryons). This characteristic that quarks can exist only in the form of colorless combinations is called *color confinement*. The confinement of gluons limits the range of the strong interaction to a few femtometers, although at high energy densities and temperatures the strong bond between quarks and gluons weakens, allowing colored partons to propagate over longer distances. This was likely the situation in the early universe as well.
The quasistatic potential between two quarks within a hadron can be parametrized in the following form:

$$V_S = -\frac{4}{3}\frac{\alpha_S}{r} + Kr \tag{1.2}$$

The Coulomb-type term dominates at small distances. It is not divergent, as α_S is not constant, but decrease with decreasing distance. This makes the radius of hadrons finite, as an equilibrium position is reached. The second term, which linearly increases with the distance r between the two quarks, gives rise to an elastic-type force. It is related to the interaction between gluons and manifests itself by the confinement of quarks within hadrons. The effect of this term is illustrated in figure 1.4 [5], [6].

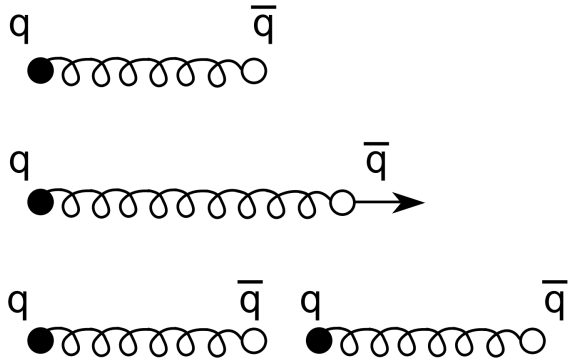

Figure 1.4: The interaction between two relatively distant quarks can be thought as an elastic force: when they reach a separation distance of around 10^{-15} m (the diameter of an hadron), the strong interaction becomes so great that new quark-antiquarks pairs are produced. Note that the springs in the figure does not represent gluons, but rather the elastic force.

1.3 Quark-Gluon Plasma

Shortly after the idea of asymptotic freedom was introduced, researchers realized its fascinating consequence for the properties of hot and dense matter, and the fact that the discovery of asymptotic freedom paved the way to our current understanding of the evolution of the early universe. For a few millionths of a second, about 10^{-6} s after the Big Bang, the universe was filled with an incredibly hot, dense soup made of all kinds of particles moving at near light speed. This mixture was dominated by quarks and gluons. In those first evanescent moments of extreme temperature, however, quarks and gluons were only weakly bound, free to move independently in a state known as quark-gluon plasma (QGP). This phase lasted until the QGP transitioned to hadronic matter, a condition that happened at around $T \approx 200\,\text{MeV} \approx 10^{12}\,\text{K}$ and lead to the formation of the ordinary matter we are familiar with nowadays. This transition is related to the spontaneous breaking of the chiral symmetry in the theory of strong interactions.
To recreate these early-universe conditions, powerful accelerators collide massive ions, such as lead nuclei. In these heavy-ion collisions the hundreds of protons and neutrons in two such nuclei smash into one another at energies of the order of $1\,\text{TeV} - 10\,\text{TeV}$. In these collisions, the formed quark-gluon plasma instantly cools, and the partons recombine into ordinary matter which rapidly go away in all directions.
The extreme conditions of the QGP-hadronic matter transition occur also in the core of neutron stars. A potential phase diagram is depicted in figure 1.5 [7, 8].

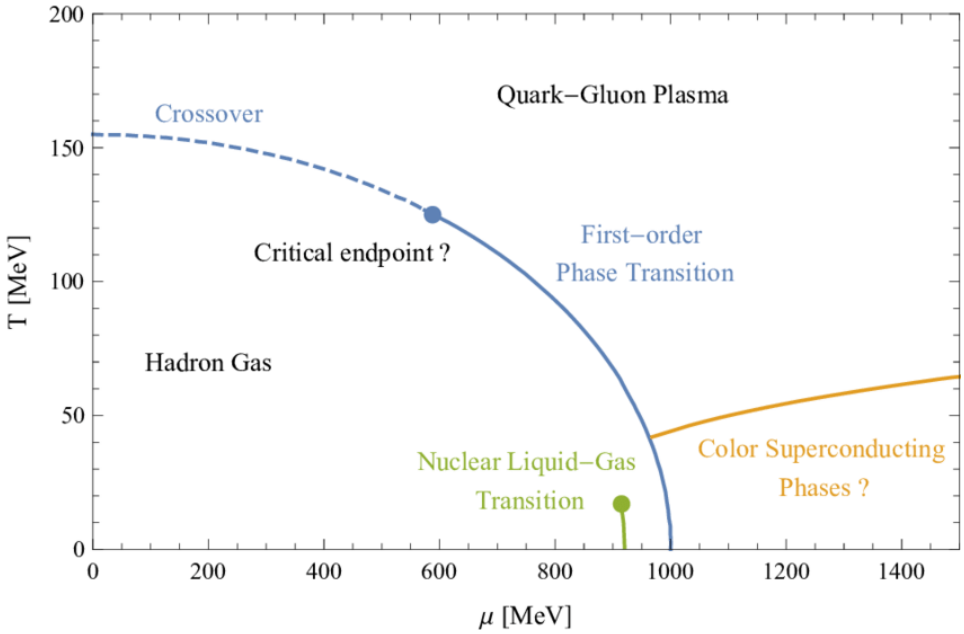

Figure 1.5: Schematic representation of QCD phase diagram. The baryochemical potential μ_B is the energy needed to increase the baryon number by one unit at fixed volume and entropy of the system and is proportional to the net baryon density of the system.

1.3.1 Role of heavy flavor hadrons

Despite the fact that we have a good qualitative understanding about the space-time evolution of the system, there are many open questions when it comes to a quantitative analysis. Heavy flavor hadrons have turned out to be an almost ideal probe to study the time evolution of the QGP due to the following reasons:

- Charm and beauty quarks are produced predominantly via hard-scattering processes in the early stages of the nucleus-nucleus collisions. In fact, due to their high mass, charm and beauty quarks can't be produced from QGP interactions, but only by hard collisions of the partons that belong to the colliding nuclei. These quarks experience the full system evolution, so in the end the heavy-flavor hadrons containing a c or b quark carry a memory of their interaction history.

- The heavy quarks masses ($m_c = 1.5\,\text{GeV}$ and $m_b = 4.5\,\text{GeV}$) are much larger than the QCD cutoff (energy threshold below which pQCD cannot be applied), which is $\Lambda_{QCD} \approx 300\,\text{MeV}$. Therefore their production can be well described by perturbative QCD.

- The heavy quarks mass is much larger than the typical temperature of the QGP medium, which is about a couple hundred of MeV, estimated by the spectrum of

directly produced photons. Consequently, the mass of heavy quarks changes a little in the hot medium and their number is conserved during the evolution.

In addition, measurements of the production of charm hadrons in high-energy hadronic collisions provide important tests for calculations based on pQCD. Moreover, investigations of the production ratios of different hadron species as a function of the transverse momentum can shed light on the charm-quark hadronisation mechanism. With these advantages, heavy flavor physics has attracted a lot of attention from both the theoretical and experimental communities and several models have been advanced to describe the heavy flavor observables [9, 10].

1.4 Evolution of heavy-ion collisions: hadronisation of the QGP

Collisions of heavy-ions with ultra-relativistic energies are used to create the QGP in the laboratory. The evolution of a heavy-ion collision is commonly described in terms of a series of stages:

1. Initial state, defined by the wave functions of the projectiles, which are universal and independent of any specific scattering process.

2. Large-Q^2 (Q^2 being the four momentum transfer squared) interactions of partons: high momentum gluons and high momentum mass quarks are created. As they have short wavelengths, they will interact with other quarks and gluons on a microscopic level.

3. Smaller-Q^2 interactions generating a pre-equilibrated parton gas.

4. Equilibrium and explosive expansion of the QGP that reaches the pseudo-critical level of the transition ($\approx 0.5\,\mathrm{GeV/fm^3} - 1\,\mathrm{GeV/fm^3}$)

5. Hadron formation, the QGP transitions to a hadron gas. The hadronisation involves quarks and gluons processes characterised by small momentum transfers and hence large values of the strong coupling costant, such that a perturbative approach is not applicable. Thus phenomenological models come into play to explain the process. At LHC energies the hadronisation occurs $7\,\mathrm{fm/c} - 10\,\mathrm{fm/c}$ after the initial collision.

6. Chemical freeze out of hadrons: after hadronisation, the created hadrons can still interact via inelastic processes, implying that the overall chemical composition can evolve further, until the temperature of the chemical freeze-out is reached. At this point, particle composition is fixed but elastic interactions can still continue.

7. Hadronic interactions that subsequently freeze-out kinetically, which is achieved at the time t of $t \gtrsim 10\,\mathrm{fm/c}$. At this point, the particle momenta are fixed.

8. The system vanishes into free-streaming of particles that propagate towards the detector, where they will be measured $\approx 10^{15} fm/c$ after the initial collision.

Before they interact, the nuclei at the LHC will be highly Lorentz contracted. The impact parameter b is the distance between the centres of the colliding nuclei. It is closely related to the number of nucleons in the nuclei that participate in an inelastic interaction. Nucleons not participating in the collision are defined as spectators, and continue travelling approximately along the beam direction after the collision. For the initial state of any given collision the multiplicity, which simply is the addition of the number of charged hadrons in a broad momentum range, can be determined. When b is small the multiplicity is high and the collision is referred to as central, while collisions with large impact parameters are labeled as peripheral. The high-energy beams of the

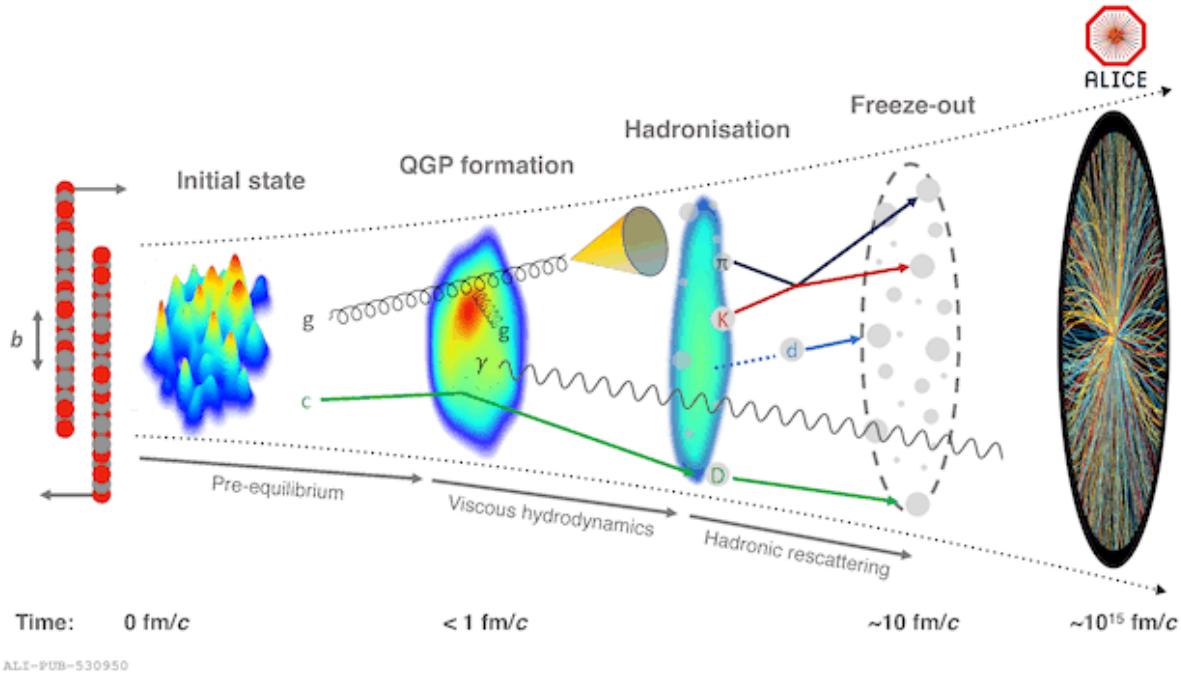

Figure 1.6: The evolution of a heavy-ion collision at LHC energies. The yellow cone indicates the parton fragmentation processes, that lead to jets, partonic showers that arise from these high energy partons, and eventually fragment into experimentally observable hadrons. Figure taken from [11].

LHC provide an unprecedented opportunity to study QGP in the laboratory, with the highest centre of mass energy in Pb-Pb collisions achieved of 5.02 TeV. This in principle allows for the hottest, densest, and longest ever lived QGP formed in the laboratory

to be probed using the ALICE detector. Also proton-proton collisions have provided opportunities for studying QCD interactions in few-body systems.

1.4.1 Small systems and searches for thresholds of QGP formation

Proton-proton collisions, together with collisions of p-Pb were originally conceived as essential references for the ultra-relativistic heavy-ion collisions. These simpler systems provide opportunities to investigate QCD in few-body systems. For instance, inclusive and heavy-flavour jet cross sections offer a way to test perturbative QCD, while measurements of the production of identified hadrons can be used to test the universality (collision-system independence) of parton-to-hardon fragmentation functions (FFs). In addition, these collisions provide insights into the thresholds for QGP formation.
Unlike heavy-ion collisions, high multiplicity events in pp collisions are not expected to result from a trivial increase in the amount of colliding matter, for example by decreasing the impact parameter b: there are always only two nucleons that participate in the interaction. Instead, high multiplicity events may be associated with energy densities high enough that allow the formation of QGP. Indeed, the highest number of particles produced in such collisions are comparable to peripheral heavy-ion collisions at lower energies, where QGP is known to form. However, it is not clear a priori whether and to what extent QGP effects are present in these events, therefore more specific measurements are needed to further explore the underlying physics [11].

1.5 Heavy flavor hadronization in pp collisions

Measurements of heavy-flavour (i.e. charm and beauty) hadron production in ultra-relativistic pp collisions provide fundamental tests of perturbative quantum chromodynamics calculations. For instance, the QGP is not expected to exist in small hadronic collision systems, however, some features like the enhancement of baryon production similar to Pb-Pb collisions has been observed in pp collisions. These phenomena challenge our current understanding of QGP formed only in nucleus-nucleus collisions and of charm hadronisation.
The transverse momentum (p_T) differential production cross section of heavy-flavour hadrons is usually calculated in QCD by the factorization into three separate components.

1. The first ingredient correspond to the distribution functions of quarks and gluons (PDFs), which describe the probability distributions of the parton momentum fractions in the proton.

2. The second term is the cross section for the partons in the protons to produce a charm or beauty quark, which defines the scattering probability calculated as a perturbative series expansion in the strong coupling constant (α_s). As m_c and m_b are much larger than $\Lambda_{\rm QCD}$ the cross section can be calculated using pQCD.

3. The third ingredient take into account the hadronisation and corresponds to the fragmentation function (FF), which parametrises the non-perturbative transition of a heavy quark into a hadron. It characterises the hadronisation of a quark to a specific hadron species. The FFs cannot be calculated with pQCD, but luckily it has been shown that they should be universal, i.e. independent of the collision system. Therefore they can be determined from measurements in e^+e^- collisions and are then applied in cross section calculations. Although, with the last experimental results, the universality of FFs has been put into discussion.

Hadron-to-hadron production ratios within the charm sector, like Λ_c^+/D^0, are useful to probe hadronisation effects, since in theoretical calculations the first two points are common to all charmed hadrons so their effects almost fully cancel in the yield ratios.
Fragmentation functions describe the probability that a hadron is created from a parton with large momentum in the vacuum. However, several puzzling observations lead to the conclusion that the fragmentation process is not sufficient to explain hadron production in high energy pp/heavy-ions collisions at the energies reached by LHC. Actually it is not a surprise that a hadronisation picture that assumes a single parton fragmenting in the vacuum has to fail: the vacuum fragmentation starts by producing additional partons through radiation, but in the environment generated by heavy-ion (and maybe also by high multiplicity pp collisions), a hot and very dense fireball of deconfined quarks and gluons is created, so the formation of bound states can directly start from the medium partons themselves.
Another hadronisation mechanism that needs to be taken into account is recombination, also known as coalescence, in which quarks that are close to each other in phase space, can simply recombine into hadrons with transverse momentum equal to the sum of the momenta of the initial partons, as shown in figure 1.7. Recombination models are built on the assumption that quarks can be treated as effective degrees of freedom having a dynamical mass approaching the constituent mass, while gluons disappear as dynamical degrees of freedom and are converted into $q\overline{q}$ pairs. The probability of finding two or three partons close together in phase space decreases as the transverse momentum of the final state hadron increases. Consequently, the recombination process is expected to dominate over fragmentation at low and intermediate p_T (up to few GeV/c), while at higher momenta fragmentation is the main phenomenon. The transition where fragmentation starts to prevail over recombination is expected to take place at higher values of p_T for baryons as compared to mesons and this insight can explain the experimental results that see an enhancement of baryons over mesons at intermediate p_T. In addition,

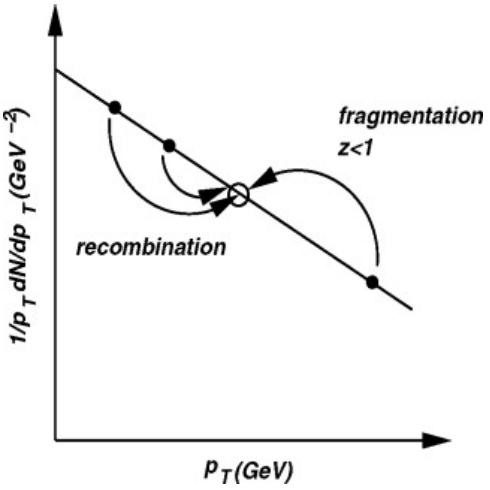

Figure 1.7: The competing effects of recombination and fragmentation on a final-state p_T distribution are shown.

recombination plays a larger role in central collisions, as they more greatly favor the transition to QGP, while fragmentation is typically seen in peripheral collisions.

1.5.1 Experimental results of charmed hadrons in pp collisions

In this section is shown that calculations using FFs tuned on e^+e^- collision data, do not adequately describe the production of charm baryons at midrapidity in pp collisions at the LHC. Instead, the measurements can only be described by model calculations that account for novel hadronisation mechanisms. In contrast, meson ratios are consistent with results from e^+e^- collisions [12].

Many models that explain the current experimental result had arisen, but the available precision of the data is insufficient to fully distinguish between the pictures. It is particularly interesting to extend the measurements of the baryon-to-meson ratio Λ_c^+/D^0 down to lower transverse momenta, as this allows for a comparison with theoretical predictions in a kinematic region where the models calculations differ from each other.

Figure 1.8 shows the $\frac{\Lambda_c^+}{D_0}$ ratio as a function of p_T at midrapidity ($|y| < 0.5$) in pp collisions at $\sqrt{s} = 13\,\mathrm{TeV}$ measured by the ALICE experiment at LHC. In the top panel, the ratio measurements taken at different center of mass energies are reported, while in the bottom panel the experimental points are compared with several model calculations. The measured $\frac{\Lambda_c^+}{D_0}$ ratios show significant deviations from the values measured in e^+e^- and e-p collisions, with an enhancement in the yield ratio up to a factor 2-5 for $p_T < 8\,\mathrm{GeV/c}$. The Monash tune of PYTHIA, that adopts hadronisation fractions based on FFs from

e^+e^- collisions, underestimates the production rates of Λ_c^+ baryons by a factor of 2 to 10, depending on p_T in the region $p_T < 12\,\mathrm{GeV/c}$.

Several models that correctly predicts a relative increase of charmed baryon production compared to mesons in pp collisions at LHC have been proposed in recent years, including: PYTHIA8 with color reconnection, SHM+RQM (statistical hadronisation model with relativistic quark model) and the Catania and QCM model, that implement quark recombination. Instead the POWLANG model, that assumes the formation of a small, deconfined, and expanding fireball in pp collisions qualitatively describe the data, but especially in the interval $0 < p_T < 1$ GeV/c POWLANG tends to underestimate the measurement.

Overall the current precision and granularity of the measurements does not discriminate among the model calculations that describe charm hadronisation at the LHC employing new mechanisms, but they confirm the baryon-to-meson enhancement compared to e^+e^- results.

In the end, the results indicate that the measured Λ_c^+/D^0 ratios at midrapidity in pp collisions at $\sqrt{s} = 5.02$ TeV and 13 TeV are described by the predictions provided by these model calculations and are compatible within uncertainty. Thus, with the current uncertainties, no significant energy dependence is observed in pp collisions at midrapidity at the LHC. [12, 13].

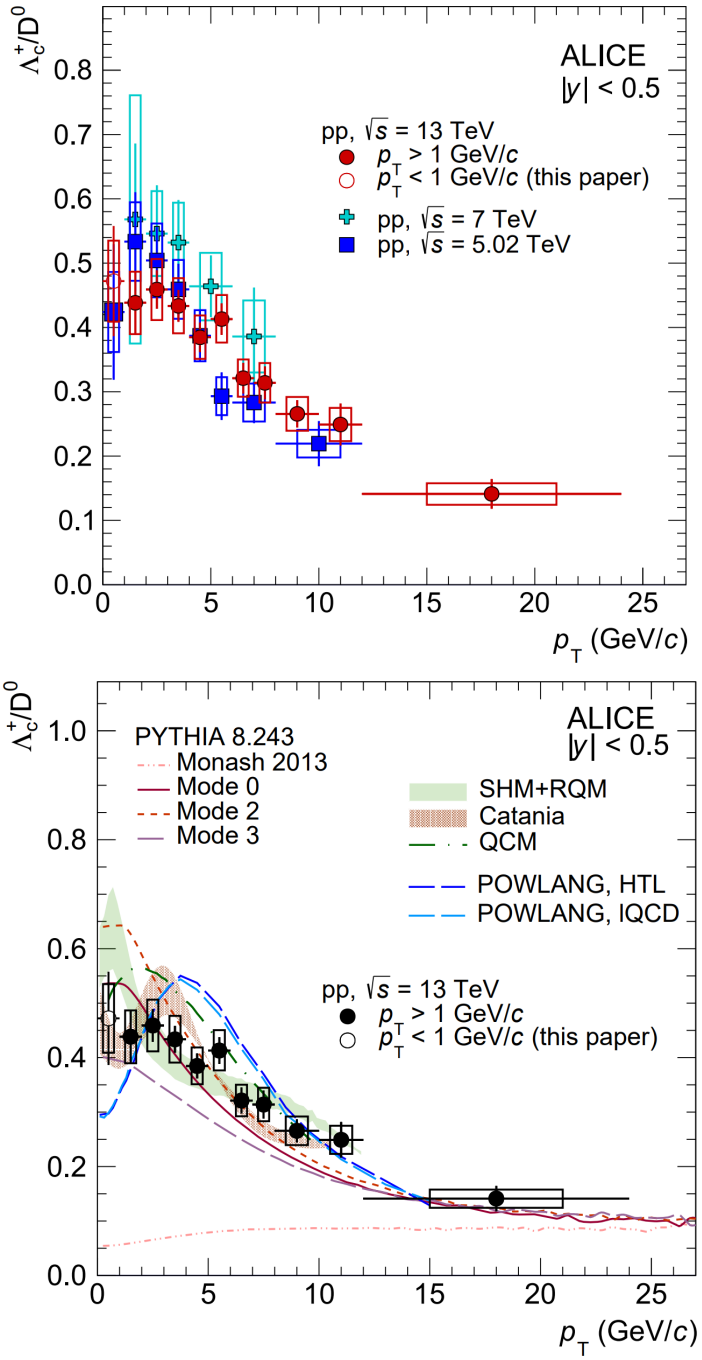

Figure 1.8: Top panel: ratio between the p_T-differential production cross sections at midrapidity ($|y| < 0.5$) of prompt Λ_c^+ baryons and D^0 mesons in pp collisions at $\sqrt{s} =$ 5.02 TeV, 7 TeV and 13 TeV. Bottom panel: ratio between the p_T-differential production cross sections at midrapidity of prompt Λ_c^+ and D^0 mesons in pp collisions at $\sqrt{s} =$ 13 TeV compared with the prediction from PYTHIA8 Monash tune, PYTHIA8 CR-BLC Mode 0, 2 and 3, SHM+RQM, Catania, QCM and POWLANG models. Figures taken from [12].

Chapter 2

ALICE: A Large Ion Collider Experiment

The ALICE experiment was proposed in 1993, to study strongly-interacting matter at extreme energy densities and temperatures. The aim is analyse the QGP, a deconfined state of quarks and gluons created in heavy-ions collisions. At the same time ALICE is studying proton-proton and proton-nucleus collisions both as a comparison with nucleus-nucleus collisions and in their own right and specific aspects of pp physics gained progressively more importance with time [11].

In 2021, ALICE completed a significant upgrade of its detectors to further enhance its capabilities and continue its scientific journey at the LHC in Run 3 and 4, until the end of 2032. At the same time, upgrade plans are being made for ALICE 3, the next-generation experiment for LHC Runs 5 and 6.

2.1 LHC

The accelerator complex at CERN (visible in figure 2.1) is a succession of machines designed to progressively increase the beam's energy. Each machine injects the beam into the next one, which takes over to bring the beam to an even higher energy, and so on. The last element of this chain is LHC (Large Hadron Collider), the world's largest and most powerful particles accelerator in the world. The construction of the LHC was approved in December 1994. LHC re-uses the tunnel that was built for CERN's previous big accelerator, LEP, dismantled in 2000.

Among the main goals of LHC there is the study of Higgs boson in detail, the search for evidence of supersymmetry, that could provide a unified description of all the fundamental forces, the exploration of matter-antimatter imbalance, trying to access dark

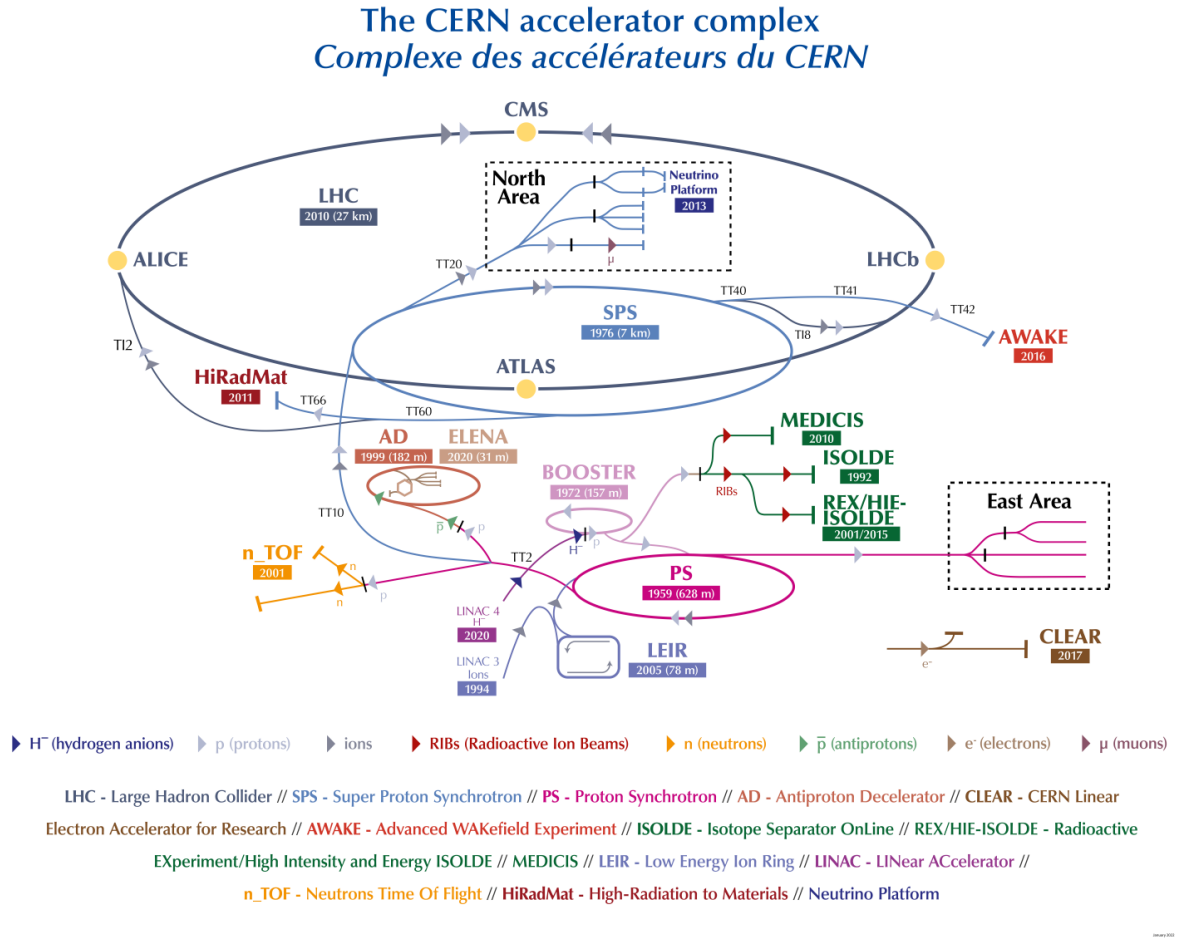

Figure 2.1: The accelerator complex at CERN.

matter and dark energy and study the quark-gluon plasma.

At the LHC, the particles form two beams that are accelerated up to the total collision energy of 5.36 TeV per nucleon pair ([14]) and 13 TeV for protons and collide at four points where the four main experiments (ALICE, ATLAS, CMS and LHCb) take place. ALICE focuses on measuring and analysing lead-ion collisions for studying QGP. ATLAS and CMS are general-purpose detectors designed to cover the widest possible range of physics, while LHCb is specialized in the study of the asymmetry between matter and antimatter present in interactions involving bottom quarks.

The hadrons in the LHC circulate around the ring in well-defined bunches. Under nominal operating conditions, each proton beam consists of 2808 bunches, with each

bunch containing about 10^{11} particles. As the bunches circulate they are squeezed and expanded along the ring, with the size varying from a few centimetres long and a millimeter wide when far from a collision point, to being squeezed up to 20 µm near a interaction point to optimize the collisions chances. Inside the collider, particles travel around in a vacuum tube and are guided using a strong magnetic field (up to 8.3 T) generated and maintained by superconducting electromagnetic devices. In particular, dipole magnets are responsible for bending and tightening the particles' trajectory, so that the beams remain stable and aligned, while quadrupole magnets focus the beam before it enters in a detector. Magnets are also employed for particle detection, for example through the amount of deflection caused by the magnetic field in the detector.

The LHC's main magnets operate at superfluid helium temperature of 1.9 K. Cryogenic techniques are used to cool the superconducting magnets and, in particle detectors, they are in charge of keeping heavy gases such as argon or krypton in a liquid state for particle detection, for example in calorimeters. One of superfluid helium's remarkable properties is its very high thermal conductivity, making it an excellent coolant.

The collider also has tree separate vacuum systems: one for the beam pipes, ensuring that the beams doesn't collide with gas molecules inside the accelerator, while the other two are for the insulation of the cryogenically cooled magnets and the helium distribution line. For the latter two cases vacuum act as a thermal insulator, to minimize the amount of heat from the surrounding room-temperature environment to the cryogenic parts, that are kept at 1.9 K. The insulating vacuum has a pressure equivalent to 10^{-6} mbar, while in the beam pipes there is an ultra-high vacuum, with a pressure of the order of $10^{-10} - 10^{-11}$ mbar, a vacuum almost as rarefied as that found on the surface of the Moon [15].

2.2 Overview of ALICE

Being the only detector specifically devoted to QGP studies, ALICE was designed to access a large number of specific observables in a wide transverse momentum range, in order to shed light on the various stages of the evolution of the heavy-ion collisions, from the initial state to the QGP phase to the mechanism that confine quarks and gluons into hadronic matter.

ALICE is optimized for the physics requirements and experimental conditions expected in nucleus-nucleus collisions at the LHC. The most stringent design constraint is the extreme particle multiplicity, with a range of several thousands of tracks produced by heavy-ion collisions. Also a large dynamic range is required for momentum measurement, spanning more than three orders of magnitude from tens of MeV/c to over 100

GeV/c. Particle Identification (PID) over much of this momentum range is essential and basically all the known PID techniques are employed in ALICE. With respect to ATLAS or CMS, ALICE is slow in acquiring data, for its nature it is focused on precision, and hopes to discriminate the thousands of particles produced by pp or heavy-ion collisions. Indeed, it provides excellent capabilities in tracking, for primary and secondary vertex reconstruction.

The overall dimensions of the detector are $16 \times 16 \times 26$ m^3 with a total weight of approximately 10000 tons. An overview of the detector with its subdetectors is shown in figure 2.2. It consists of two main parts: the central barrel, which measures hadrons,

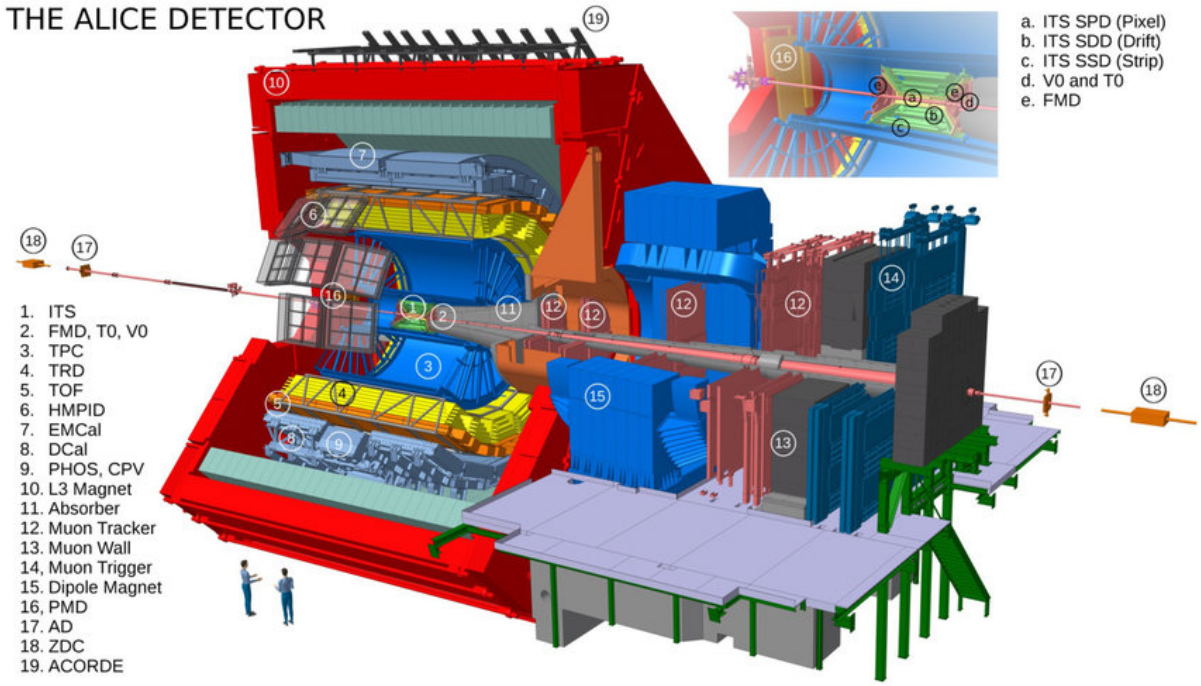

Figure 2.2: The ALICE experimental apparatus with the names of the main sub-detectors.

electrons, and photons, and a forward muon spectrometer. The central part covers polar angles from 45° to 135° and is embedded in a large solenoid magnet. From the inside out, the barrel detectors include:

1. Inner Tracking Systems (ITS)
2. Cylindrical Time-Projection Chamber (TPC)
3. Transition Radiation Detector (TRD)

4. Three particle identification arrays of Time-of-Flight (TOF)
5. The High Momentum Particle Identification Detector, a ring imaging Cherenkov (HMPID)
6. The Electromagnetic Calorimeter (EMCal)
7. The Photon Spectrometer (PHOS)

All detectors expect HMPID and the two calorimeters cover the full azimuth angle. The forward muon arm, that covers the range from 2° to 9° consists of a complex arrangement of absorbers, a large dipole magnet, and fourteen planes of tracking and triggering chambers. Moreover there are several smaller detectors for global event characterization and triggering located at small angles and an array of scintillators (ACORDE) used to trigger on cosmic rays.
A detailed overview of ALICE, its performances and results can be found in Refs. [15, 16].
In the following sections, only the detectors that measured the variables used in this analysis are described.

2.3 ITS: Inner Tracking System

The Inner Tracking System, whose layout is pictured in figure 2.3, is a cylindrically-shaped silicon tracker that surrounds the interaction region. It consists of six layers, with radius ranging from 4 cm to 43 cm, covering the pseudo-rapidity range $|\eta| < 0.9$. The outer radius is determined by the necessity to match tracks with those from the TPC, and the inner radius is the minimum allowed by the size of the beam pipe. The main tasks of the ITS are:

- Determination of the primary vertex with a high resolution, better than 100 micrometer.
- Reconstruction of secondary vertices, where short-lived hadrons like Λ_c^+ decay.
- Tracking and identification of particles with low-momentum (below 200 MeV/c) that are missed by the TPC.
- Improve the momentum and angle resolution for particles reconstructed by the TPC.

The ITS is made up of six layers of silicon detectors. Because of the high particle density in heavy-ion collisions, the innermost two layers, where there are about 50 particles per cm^2, are composed of Silicon Pixel Detectors (SPD), responsible for determining the

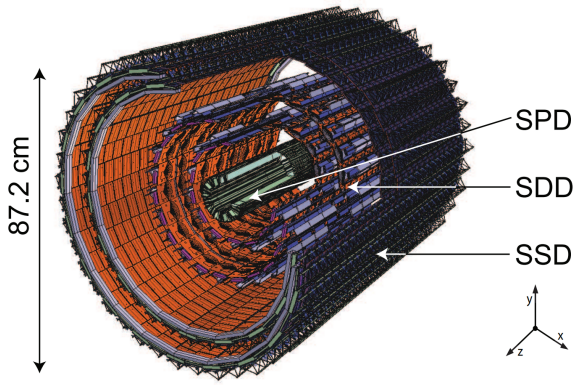

Figure 2.3: Layout of the ITS. The beam line is along the z direction.

position of the primary vertex. For the following two layers Silicon Drift Detectors (SDD) were chosen and double-sided Silicon micro-Strip Detectors (SSD) for the two outer layers, where the track density is expected to be below one particle per cm^2. The four outer layers have analogue readout and therefore can be used for particle identification by measuring $\frac{dE}{dx}$ in the non relativistic region. To measure the separation between the interaction and the secondary vertex (that is the decay vertex of heavy flavoured hadrons) the ITS provides a resolution on the track impact parameter of the order of few tens of μm, although this is not always sufficient, as for the case of the Λ_c^+ baryon [17].

2.4 TPC: Time Projection Chamber

The Time Projection Chamber (TPC) is a device that uses a combination of electric and magnetic fields, together with a volume of gas, to perform a three-dimensional reconstruction of the particle's track. A negative high-voltage electrode plane located at the centre divide the chamber in two halves and establishes a uniform electric field **E** from the two ends to the centre that accelerate the electrons towards the endplates. The strong magnetic field **B** is aligned in one direction and therefore is parallel and antiparallel to **E** in the two sections of the chamber.

The ALICE TPC (whose schematic is shown in figure 2.4) is the central tracking detector, with an active volume that has an inner radius of about 85 cm, an outer radius of about 250 cm and an overall length along the beam direction of 500 cm. It is supplied with a uniform electrostatic field of 400 V cm^{-1} and a 0.5 T magnetic field. The gas inside the detector, a Ne-CO_2-N_2 mixture at atmospheric pressure, is ionized by charged particles traversing the detector. The formed electrons from ionisation drift under the influence of the electric and magnetic field making a helical trajectory towards the endplates of

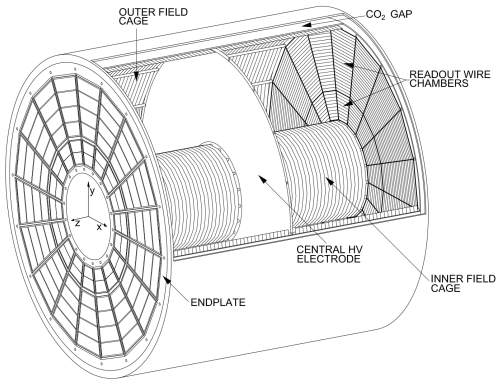

Figure 2.4: Schematic of the TPC, figure taken from [18].

the cylinder, which are segmented layers of proportional counters. The measurement of the arrival point and time of the electrons give a three-dimensional image of the original particle track, and the momenta can be estimated from the track curvature. The ALICE TPC is specifically designed to measure tracks with transverse momentum ranging from 0.1 GeV/c to 100 GeV/c. It takes into account that each lead nuclei collision produces approximately 10^4 charged particles, which traverse the TPC at nearly the speed of light. The TPC offers excellent spatial resolution, though it requires longer dead time compared to other detectors. It also has remarkable PID capabilities, with a resolution better than 5%, via the information of the specific energy loss, $\frac{dE}{dx}$ (an example is shown in figure 2.5), described by the Bethe-Bloch formula [18].

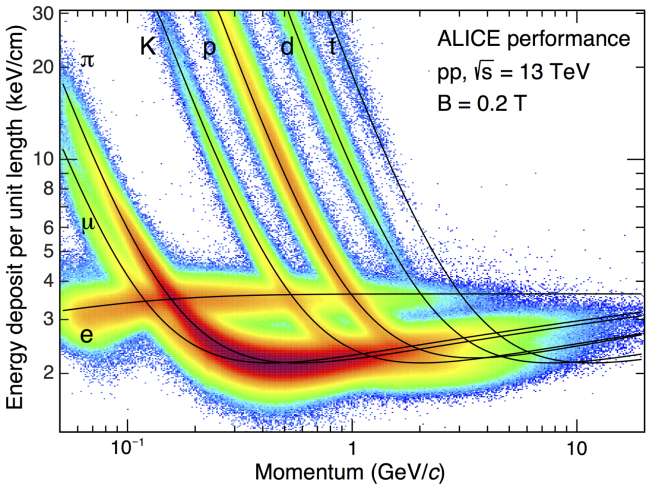

Figure 2.5: Specific energy loss ($\frac{dE}{dx}$) versus particle momentum in the TPC in pp collisions at $\sqrt{s} = 13\,\text{TeV}$. The solid lines represent the expected trends for different particle species, according to the Bethe-Bloch formula.

2.5 TOF: Time Of Flight

The Time Of Flight is an essential system for particle identification, that can provide the speed of any charged particle by measuring the travelling time t over a known distance L. This information is then combined with the momentum p, obtained with other detectors, to calculate the particle's mass:

$$\beta = \frac{v}{c} = \frac{L}{tc} = \frac{1}{\sqrt{\left(\frac{mc}{p}\right)^2 + 1}} \longrightarrow m = \frac{p}{c}\sqrt{\frac{c^2t^2}{L^2} - 1} \tag{2.1}$$

Specifically, in ALICE the TOF system covers a cylindrical surface of 141 m^2 with an inner radius of 3.7 m, a pseudorapidity range of $|\eta| < 0.9$ and a full azimuthal coverage. It is designed to identify charged particles with an intermediate momentum range ($0.5 < p_T < 4\,\mathrm{GeV/c}$) and in order to accomplish this, the TOF exploits the Multigap Resistive Plate Chamber (MRPC) technology, capable of an intrinsic time resolution better than 50 ps with an efficiency close to 100%. The whole system, illustrated in figure 2.6, is made of 1593 MRPCs, subdivided into 18 sectors, each covering an azimuthal angle of 20°. In each MRPC there is a gas maintained at atmospheric pressure and con-

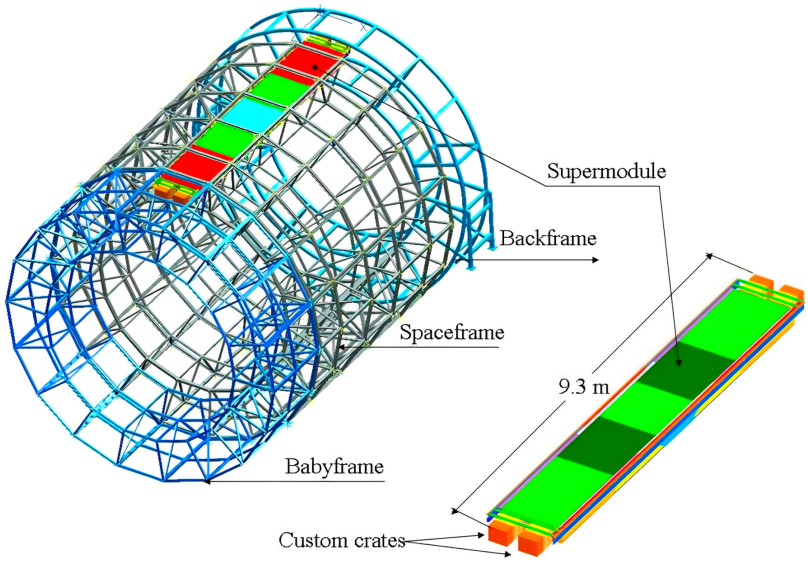

Figure 2.6: Layout of the TOF system, the MRPCs are subdivided into 18 supermodules.

tained in a narrow space between parallel plates of high resistivity, that in ALICE are made of soda-lime commercial glass. A high potential difference is maintained between the two external plates, so that when a charged particle passes through the detector it produces ionisation that is drifted towards the electrodes, producing an avalanche. The

high resistivity of the electrodes ensures that the discharge does not spread out too much. The advantage of using MRPCs instead of the standard RPCs (that consists of only two plates separated by a gas layer) is that in the MRPCs the gas gap between the electrodes is divided by means of internal plates which are physical barriers stopping the avalanche growing too big, so it is possible to apply a very strong electric field that ensures a very good time resolution [19].

The PID capabilities measured by the TOF detector in pp collisions at $\sqrt{s} = 13\,\text{TeV}$ are shown in figure 2.7 [3].

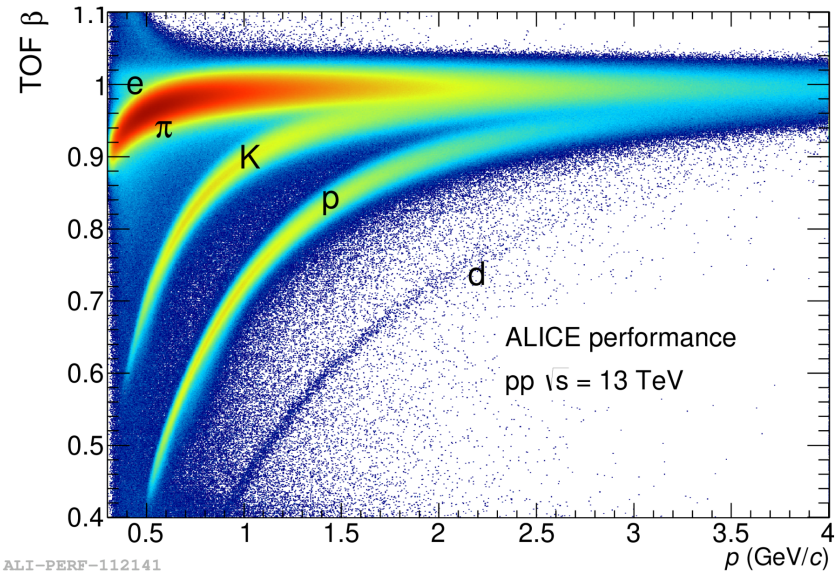

Figure 2.7: Measurements of β of charged particles by TOF as a function of momentum in pp collisions at $\sqrt{s} = 13\,\text{TeV}$.

Chapter 3

Neural networks

Machine learning is a method of data analysis that automates analytical model building by learning from data. Using algorithms that iteratively learn from data, machine learning allows computers to find hidden insights without being explicitly programmed where to look. Machine learning is used in a wide variety of topics, such as fraud detection, pattern and image recognition, recommendation engines and, most importantly, it became an essential tool for data analysis in physics.
Neural networks (represented in 3.1) are a way of modeling biological neuron systems mathematically. These networks can then be used to solve tasks that many other types of algorithms cannot. The concept of deep learning simply refers to neural networks

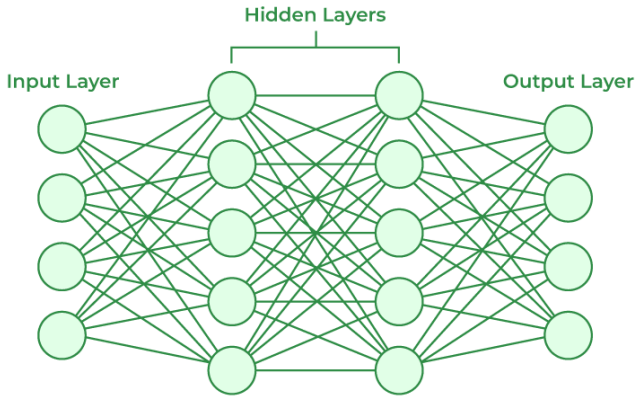

Figure 3.1: Neural network composed of many layers: the first is the input layer, the last is the output layer and those in the middle are the hidden layers.

with more than one hidden layer. There are different types of machine learning, in this thesis the supervised learning paradigm was adopted. Supervised learning algorithms are trained using labeled examples, such as a set of inputs with the corresponding cor-

rect outputs, and the algorithm learns by comparing its actual outputs with the correct ones to find errors. Then the model is modified accordingly, by adjusting the weights and bias values in the network. At the beginning, the data are splitted into two portions: the training set, used to fit a model, and a testing sample for the measurement of the goodness of the model. Is it possible to introduce also a validation set to evaluate performance and possibly optimise the network before proceeding to the testing phase [20]. In high-energy physics, simulated Monte Carlo events are frequently employed for these three samples, and the performance on the testing sample is compared against experimental data, which remains unseen during training.

3.1 Perceptron model and sigmoid neurons

The simplest artificial neuron is the so-called perceptron [21], a basic representation is showed in figure 3.2. A perceptron takes several binary inputs x_i and produces a single binary output. There are weights w_i associated to every input, expressing the importance of them, and there is a bias b, another term that is a measure of how easy it is to get the perceptron to output a 1. The weighted and biased input $w \cdot x + b$ is then passed

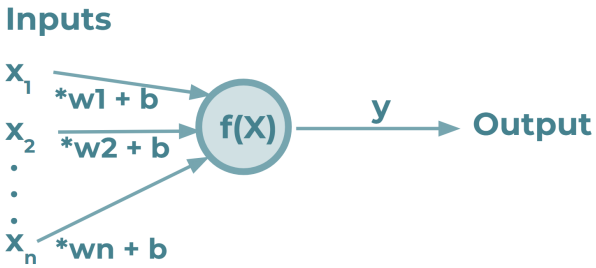

Figure 3.2: Schematic representation of the perceptron model: each input has an adjustable weights and the sum of all weighted inputs and biases is passed to the activation function $f(X)$, whose output is y.

to an activation function, that allows us to set boundaries for the overall output value and introduce non-linearity in the network. In the basic perceptron model the activation function is simply the step function (figure 3.3a) and thus the output is:

$$\text{output} = \begin{cases} 0 & \text{if } w \cdot x + b \leq 0 \\ 1 & \text{if } w \cdot x + b > 0 \end{cases} \tag{3.1}$$

Perceptrons can be used as a method for weighing evidence to make decisions and can also compute the elementary logic gate NAND and hence any logic function, thanks to the universality of NAND. Of course, perceptrons aren't just merely a new type of NAND gate, but it is possible to devise learning algorithms which can automatically tune the

weights and biases of a network of artificial neurons and thanks to this feature the use of artificial neurons open up to a whole new different and powerful way to solve problems. A slightly more complicated artificial neuron, yet more useful for understanding the learning process, is the sigmoid neuron. Each input of the sigmoid neuron can take any values between 0 and 1 and the activation function used is the sigmoid function (see figure 3.3b):

$$\sigma(w \cdot x + b) = \sigma(z) \equiv \frac{1}{1 + e^{-z}} \tag{3.2}$$

the shape of this function is basically a smoothed step function, so that small changes in the weights and bias cause only a small change in the output:

$$\Delta\text{output} \approx \sum_j \frac{\partial\text{output}}{\partial w_j}\Delta w_j + \frac{\partial\text{output}}{\partial b}\Delta b \tag{3.3}$$

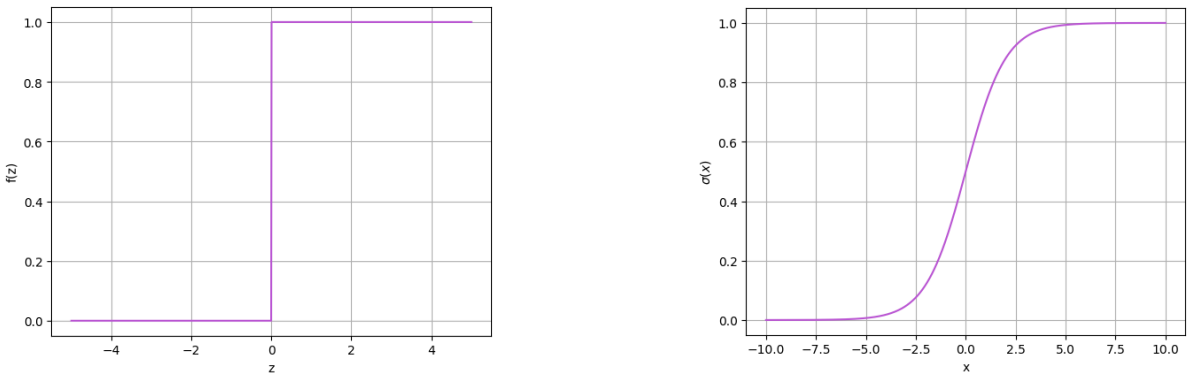

(a) Step function

(b) Sigmoid function

Figure 3.3: Two types of activation functions.

3.2 Gradient and stochastic gradient descent

The aim is to develop an algorithm that is capable of finding weights and biases so that the network's output closely matches the right answer $y(x)$ for each training input x. To assess how well this is being achieved, a cost function (or loss function) is defined, with the purpose of expressing the discrepancy between the network output and the real value. The loss function deployed in the analysis performed in this thesis is the categorical cross-entropy. It is used in multi-class classification tasks and works pretty well with the softmax activation function. The functional form is:

$$C(y, p) = -\sum_{c=1}^{N} y_c \ln(p_c) \tag{3.4}$$

where p_c is the predicted probability, y_c is the truth value and the sum is extended to all the different categories. The goal is to minimize this function and this is done by an algorithm known as gradient descent. Often the cost function has a lot of variables, and it is not tempting to use calculus and find the minimum analytically. What is done instead is repeatedly compute the gradient of the cost function ∇C and then move in the opposite direction.
The stochastic gradient descent is a variation of the classic one that can be used when the number of training inputs is very large and consequently calculating the gradient of the cost function is time and computationally consuming. In this case the training data are randomly shuffled and then divided into a whole bunch of mini-batches. The gradient is then estimated according only by the mini-batch sample. The result it is not gonna be the actual gradient of the cost function, so it is not the most efficient step downhill, but each mini batch does give a pretty good approximation, and more importantly, it donates a significant computational speedup. An epoch of the training is completed when the training inputs are exhausted.
Backpropagation is a fast algorithm for computing the gradient of the cost function. It consists simply in a smart application of the chain rule, that allows starting from the output layer to move backwards and calculate the error vector of each layer, a quantity strictly related to the gradient of the loss function.

3.3 Evaluating performances

The code for training and applying various machine learning algorithms can be written in just a few lines. After the setup, it's important to evaluate some figures of merit to get insight of the performances of our model.
The receiver operating characteristic curve, or ROC curve, is a representation of the capacity of a binary classifier to separate the two classes, as its discrimination threshold is changed. It shows the relation between the true positive rate against the false positive rate. In the context of signal and background, it typically plots signal efficiency versus background rejection (i.e. 1 -efficiency). To compare classifiers, the area under the curve (AUC), can be computed: the closer the AUC value is to 1, the better the separation is, while random guessing corresponds to an AUC of 0.5. An example is depicted in figure 3.4. Another interesting parameter to analyze is the significance S:

$$S = \frac{s}{\sqrt{s+b}} \tag{3.5}$$

where s (b) is the sum of signal (background) events. Usually the significance is computed above a cut value on the discriminant output, scanning its full range. Typically it goes through a maximum before starting to decrease when the statistics become too small. The maximum significance corresponds to the optimal value on which to cut on the

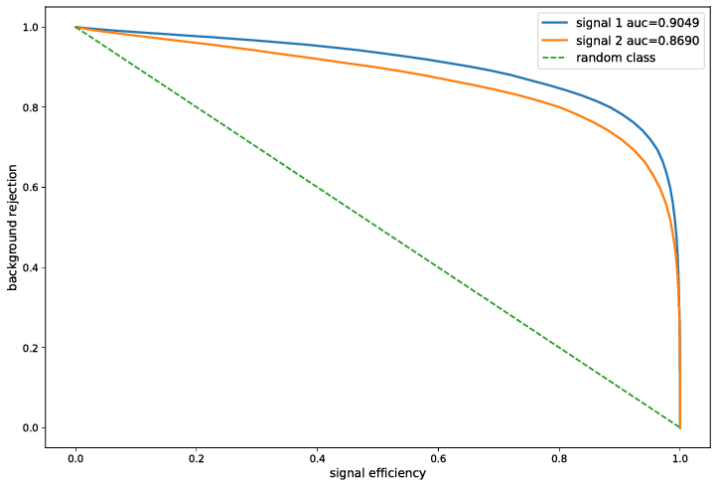

Figure 3.4: Example ROC curves. The dashed green line corresponds to random guessing.

discriminant output to get the best possible analysis, by suppressing the background by a large factor while leaving the signal events relatively intact.

Chapter 4

Λ_c^+ reconstruction

The study of the production of charmed baryon is fundamental to probe the formation of QGP and the theoretical expectations of QCD. The data provided by the ALICE experiment showed that the baryon production observed in pp collisions at the LHC can only be described by model calculations that account for novel hadronisation mechanism [12]. Determining the production of Λ_c^+ down to low transverse momenta is particularly important because we can compare the different theoretical predictions in a kinematic region where the models calculations differ from each other.
The Λ_c^+ baryon is composed of the quarks udc, with quantum numbers $I(J^P) = 0(1/2^+)$. Its mass is $2286.46(14)\,\mathrm{MeV/c^2}$ and its mean lifetime is $2.024(31) \times 10^{-13}\,\mathrm{s}$. The decay channel considered here, $\Lambda_c^+ \rightarrow pK_0^+$, illustred in figure 4.1, has a branching ratio of $1.59(8)\,\%$.

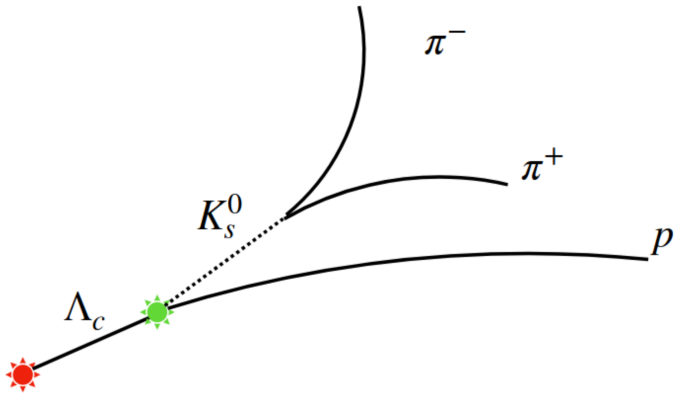

Figure 4.1: The decay considered in this analysis: $\Lambda_c^+ \rightarrow pK_s^0$, that happens for weak interaction. The K_s^0 in turn decays into two pions, also due to weak interaction: $K_s^0 \rightarrow \pi^+\pi^-$. ALICE detectors can only directly detect the two pions and the protons.

Determining how many Λ_c^+ are produced is not easy, due to the low signal to background ratio. In addition, for tracks with low transverse momentum, the spatial reso-

lution of the ITS is about 100 µm, and it is higher compared to the average distance travelled by Λ_c^+, that, due to its short lifetime, is about $c\tau \approx 60\,\mu m$. This doesn't allow to distinguish the primary vertex from the second, so to reconstruct the signal of Λ_c^+ and combine the information coming from experimental data sophisticated techniques are needed. An invariant mass analysis may be performed to determine the original particle's mass and therefore identify Λ_c^+ particles. The idea is that if the obtained value is consistent with the true mass of the decaying particle, a Λ_c^+ particle is considered detected, otherwise it is only a random combination of independent tracks. However, there is a problem with this approach: since many particles are produced in the experiment, a large background of false candidates may result in invariant masses close to the actual value, making it an intricate task to distinguish the actual Λ_c^+ signal. For this reason machine learning techniques were employed to separate the real signal of Λ_c^+ from the background, which consists of every possible combination of particles that are not products of Λ_c^+ decay, but exhibit similar features. In particular, TMVA was used to classify the events as either signal or background, where each event is a combination of particles with characteristics that are potentially compatible with a Λ_c^+ decay.

4.1 Tensorflow and Keras

TensorFlow is an open source library for numerical computation and deep learning developed by Google, with TF 2.0 being officially released in late 2019. It supports various programming languages [22], although Python tends to dominate. Keras is a high-level python library that can use a variety of deep learning libraries underneath, such as TensorFlow. Due to the huge popularity of Keras, when TF 2.0 was released, Keras was adopted as the official API (Application Programming Interface) for Tensorflow [23].

4.2 TMVA

In high-energy physics multivariate classification methods based on machine learning techniques have become a fundamental ingredient to most analyses. Integrated into the analysis framework ROOT, TMVA (Toolkit for Multivariate Analysis) is a toolkit which hosts a large variety of multivariate classification algorithms [24]. All multivariate techniques in TMVA follow the supervised learning paradigm. A typical TMVA analysis, both for classification and regression tasks, consists of two independent phases: the training phase, where the multivariate methods are trained, tested and evaluated, and an application phase, where the chosen methods are applied to the concrete problem they have been trained for. Also a pre-analysis is made that calculates the correlation matrix of the input variables. Although TMVA is specifically designed for high-energy physics, its application is not limited to this field.

4.2.1 PyMVA

PyMVA is the interface of TMVA for third-party multivariate tools based on Python. It is created to make powerful external libraries easily accessible with a direct integration into the TMVA workflow. Thanks to this interface it is possible to book Keras methods, like the `Sequential` model used in this thesis.

4.2.2 Training phase

At the beginning of the program, a `Factory` object is created. The input data sets used for training and testing of the multivariate methods are passed to the Factory (TMVA supports ROOT TTree objects) and the input variables used for training are registered with the Factory thanks to the `Add Variable` method. Additionally, "spectator" variables can be defined: these are part of the dataset but are excluded from training and evaluation. Spectator variables can be useful for tasks like correlation tests. The input events are randomly split into two ROOT Trees, one dedicated to the training and the other for testing. It is possible to apply selection requirements (cuts) upon the input events, based on any variable present in the data sets. TMVA can internally renormalise the signal and background training weights such that their respective sums of effective events is equal. After, all methods are booked via the `Factory`: this concludes the initialisation of the `Factory` phase and no further specific multivariate actions are left to do. The methods are trained with the command:

```
factory->TrainAllMethods();
```

and the training results are stored in the weight files. Subsequently, the methods are tested and in the case of a signal/background classification task they provide scalar outputs according to which an event can be classified as either signal or background with the command

```
factory->TestAllMethods();
```

Finally, the performance evaluation in terms of signal efficiency, background rejection, ROC curves and other parameters is done by invoking the command:

```
factory->EvaluateAllMethods();
```

4.2.3 Application phase

The application of training results to a data set with unknown sample composition is governed by the `Reader` object. In the initialisation phase, the input variables are registered and the preferred multivariate methods are booked. As booking argument, the name of the weight files is given. The weight file provides for each of the methods full and consistent configuration according to the training setup and results.

4.3 Input data and variables

During the training phase, the data sample used for signal events were taken from pp collisions simulated by the Monte Carlo generator PYTHIA8 [25]. To optimize the statistic significance in these simulations it was required the presence of at least one Λ_c^+ decaying via the hadronic decay channel under consideration. Also the ALICE's detectors were incorporated, simulating the interactions between particles and the detector materials as accurately as possible, as well as the generation of the corresponding detector response signals. The simulation of the ALICE detector and particle propagation was carried out using the GEANT3 software [26]. The background data sample was derived from actual measurements taken by ALICE during its second data-taking phase (run 2) between 2016 and 2018 and the same data was used for the application after the algorithm has been trained and tested. During the training phase, to make sure only background data were selected, only data points that gave a reconstructed invariant mass that was outside an interval of 3σ around the known mass of Λ_c^+ were employed.

Choosing the variables that the neural network uses for training is a delicate step, since exactly these variables are the instruments to distinguish if an event is signal or background. There are two main criteria that help to determine if a certain variable is suitable for training the algorithm. The first is checking how different the variable's distributions for signal and background are: if the two distributions are significantly distinct, then the variable is good to discriminate between signal and background events. The second important aspect to consider is the presence of spurious correlations between the input variables and the prediction of the model, as in general these unwanted correlations make the model lack from robustness and generalization. In fact, the algorithm may end up relying on these spurious dependencies to classify events, leading to incorrect decisions, as the model is not learning the true distinguishing physical features of the signal. The variables tested for correlation and whose distributions in signal and background have been analyzed are listed below. In this context, the potential proton is the "bachelor" particle and the potential K_S^0 is the V^0 particle.

- **massK0S**: invariant mass of the V^0 particle. It is obtained by finding two particles coming from the same vertex with opposite charge and reconstructing the mass of the particle that generated them, with energy and momentum conservation, assuming the particles' masses are $m_\pi = 139\,\mathrm{MeV/c}$ [27]. The expected value for the signal events is the K_s^0 mass: $m_{K_S^0} \approx 497\,\mathrm{MeV/c^2}$.

- **tImpParBach**: impact parameter of the bachelor particle, defined as the minimum distance from the bachelor track and the primary vertex, on the plane that is normal to the track.

- **tImpParV0**: impact parameter of the V^0 particle.

- **ctK0S**: $c\tau$ for the V^0. The expected value for K_s^0 is approximately 2.68 cm.
- **cosPAK0S**: cosine of the angle between the reconstructed direction of V^0 and the line connecting the primary vertex to the secondary. It's expected to be close to 1.
- **nSigmapr**: this PID variable accounts for the probability, in units of standard deviations, that the bachelor particle is actually a proton, combining the information from the TOF and the TPC. According to the TOF, this probability is obtained by comparing the time it takes for the bachelor particle to reach the TOF, with respect to that of a real proton. In case of the TPC detector, this value is obtained by comparing the energy loss $\frac{dE}{dx}$ of the bachelor particle, with respect to that lost by real protons. For candidates where the TOF information is missing, because of detector's inefficiency, bad matching of the track or simply in case of low momentum particles which cannot reach the TOF inner radius due to the magnetic field, this variable is exactly the value provided by the TPC; otherwise, the value from the TOF and the TPC are summed up in quadrature.
- **dcaV0**: it is the "Distance of Closest Approach" of the V^0 particle, the reconstructed minimum distance of the two daughter particles of V^0.
- **bachelorPt**: transverse momentum of the bachelor particle.
- **V0Pt**: transverse momentum of the V^0 particle.
- **LcPt**: transverse momentum of Λ_c^+. This is used only as a cut variable, to select the momentum interval from 1 GeV/c to 2 GeV/c.
- **massLc2K0Sp**: Reconstructed mass Λ_c^+, at this stage is only used for the correlation matrix, to check the degree of correlation of the other variables to this one.
- **asymmPt**: it is a combination of `V0Pt` and `LcPt`, it has no precise physical meaning but its definition and explanation on why it is used can be found below.

The variables distribution for signal and background were plotted, results are visible in figure 4.2; to be noted that some distributions have been drawn with a logarithmic scale on the y axis.

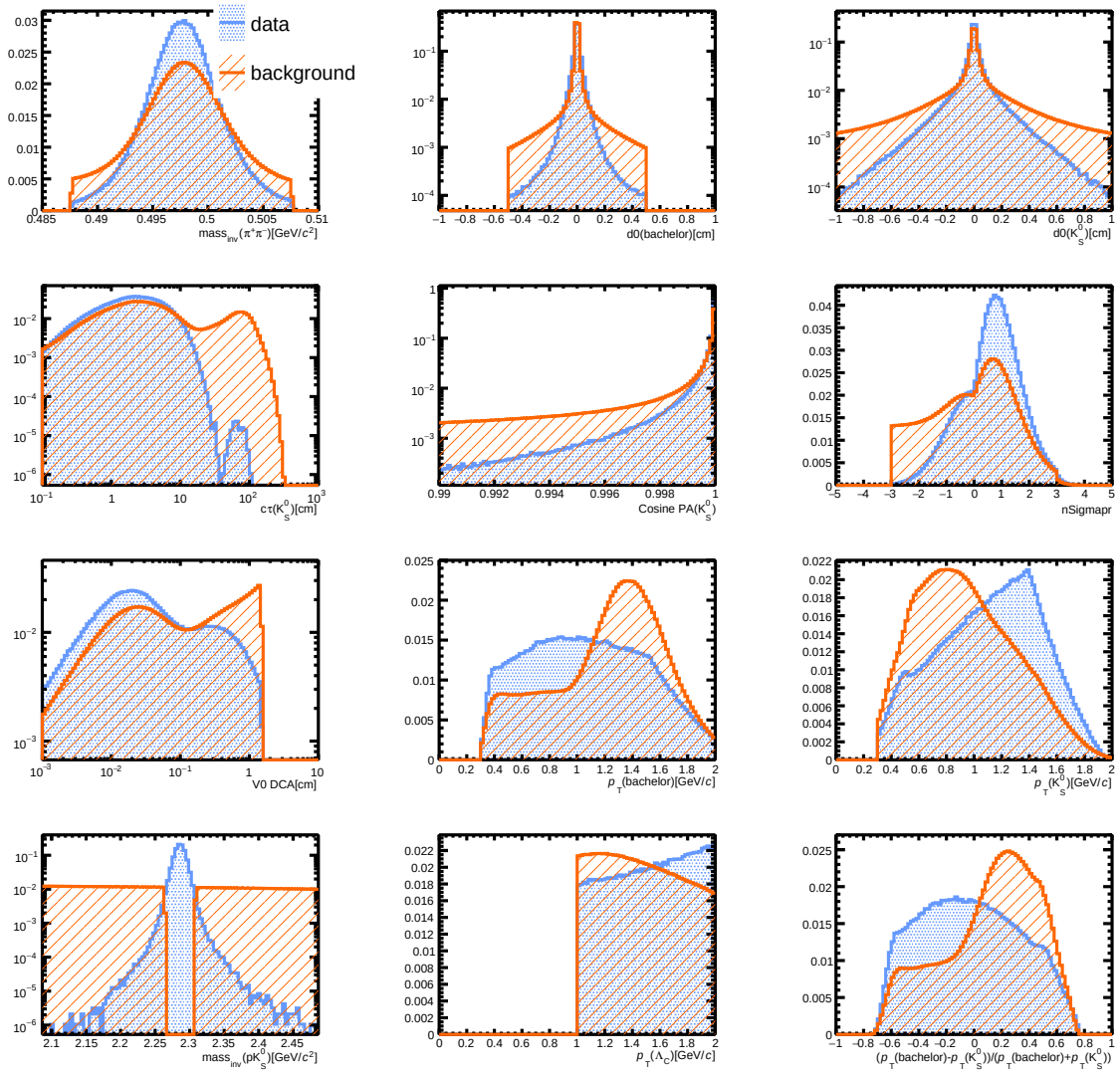

Figure 4.2: Input variables distribution in p_T range [1,2] GeV/c^2.

The transverse momentum of the bachelor, p_t(bachelor) and the V^0, $p_t(V_0)$, stand out in a remarkable shape difference between signal and background distribution. However, these variables are correlated to the transverse momentum of the Λ_c^+ up to 21-23%, as well to the Λ_c^+ reconstructed mass up to 14%, as can be seen from the correlation matrix in figure 4.3, so they are not suitable for the analysis. To overcome this problem it was introduced this new variable called **AsymmPt**, defined in the following way:

$$\frac{p_t(\text{bachelor}) - p_t(V^0)}{p_t(\text{bachelor}) + p_t(V^0)} \tag{4.1}$$

that keeps the property of having nice different distributions for the signal and back-

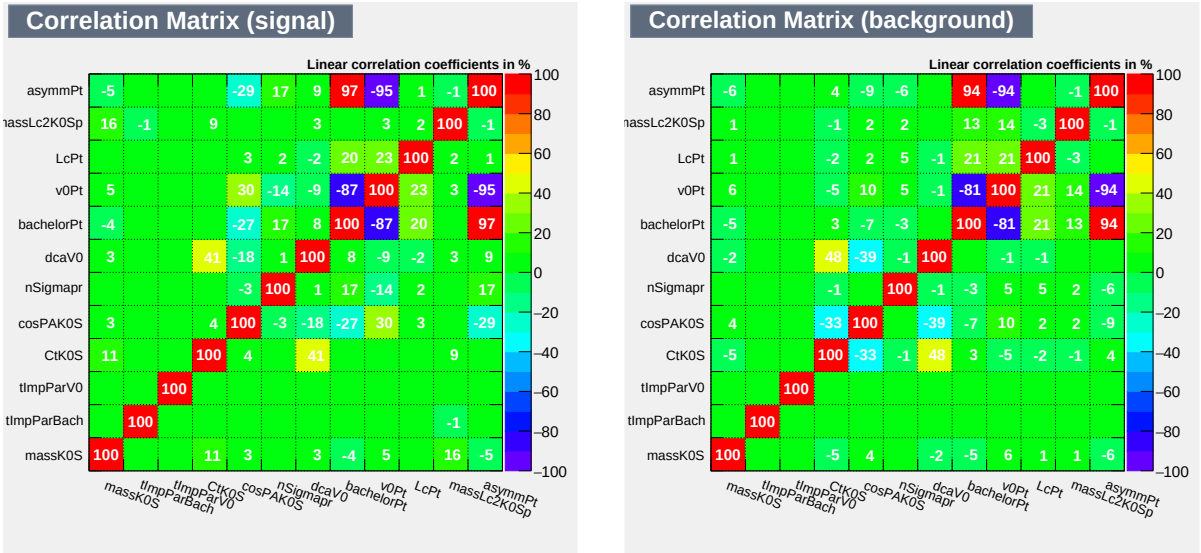

Figure 4.3: Correlation matrices of the input variables calculated on the training signal data (left) and on the training background data (right).

ground, like the transverse momentum of the bachelor and the V^0, but it is not correlated to the reconstructed invariant mass. To evaluate the positive impact of `AsymmPt`, two independent training of the model, with and without `AsymmPt`, were done and applied to the data.

4.4 Description and training of the model

The algorithm trained for the analysis was Keras `Sequential` model, imported in TMVA thanks to PyMVA (4.2.1). The following lines describe the model configuration:

```
# Define model
model = Sequential()
model.add(Dense(64, activation='relu', input_dim=7))
model.add(Dense(2, activation='softmax'))

# Set loss and optimizer
model.compile(loss='categorical_crossentropy',
              optimizer=SGD(learning_rate=0.01),
              weighted_metrics=['accuracy', ])
```

The two layers that composed the network are densely connected, meaning it is a feed-forward network where every neuron is connected to every other neuron in the next layer. The parameters inside `Dense` indicate the number of neurons and the activation function

in the layer. The first layer has the Rectified Linear Unit (ReLU) activation function, that is $f(x) = \max(0, x)$, while the second has the softmax function $S(z)$, that is defined like this:

$$S(z) = \frac{e^{z_i}}{\sum_j e^{z_j}} \tag{4.2}$$

and whose output is interpreted as a probability of a certain event to be background or signal. In the compilation of the model, the optimizer is asking how to perform the gradient descent, while the loss requires that we indicate the desired loss function. In this case, the stochastic gradient descent was computed and categorical cross-entropy was used as a cost function.

4.4.1 Controlling overtraining

Overtraining, or overfitting, is what happens when a classifier learns too much about the specific details of the training sample, while these features are not representative of the underlying distributions. This often results in low error on the training set but high error on test set, because the classifier does not generalise well. To check if the model suffered from overtraining, the classifier output distributions for the training and test set were plotted and superimposed. The response of the model is a continuous output where 0 means the model thinks has an 100% fidelity of classifying the event as background, and 1 that is 100% sure that is signal. Intermediate values represent the probability of the event of being a signal. As can be seen from figure 4.4 the are no significant differences in the two sets, so the model generalise well to unseen data. The overtraining test was performed on both the classifiers, the one trained with the variable `AsymmPt` and the one without.

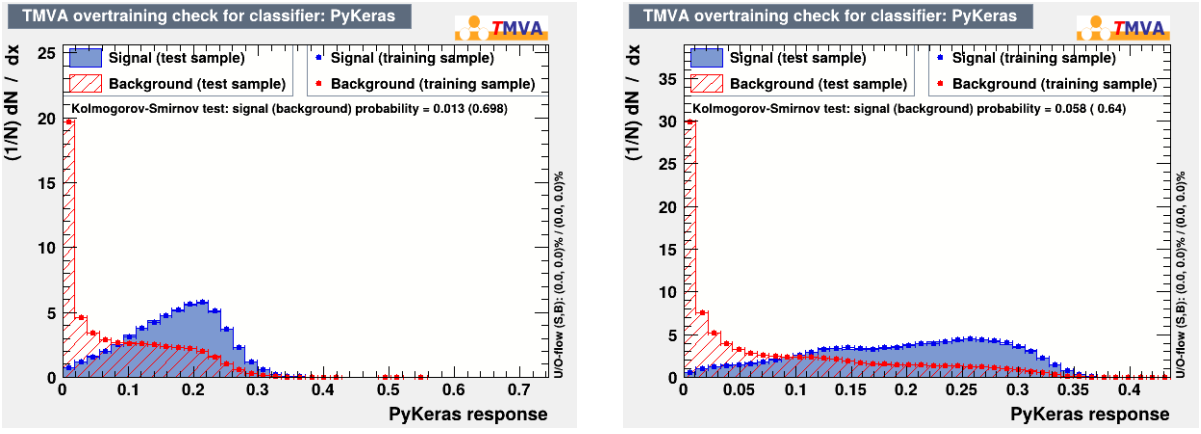

(a) (b)

Figure 4.4: Test and training output distribution, (a) without `AsymmPt`, (b) with `AsymmPt`.

4.4.2 ROC curve

In figure 4.5 the receiver operating characteristic (ROC) curves are plotted for the two classifiers. The classifier trained with the additional variable has better performances for all the range of signal efficiency, even if it is a small difference.

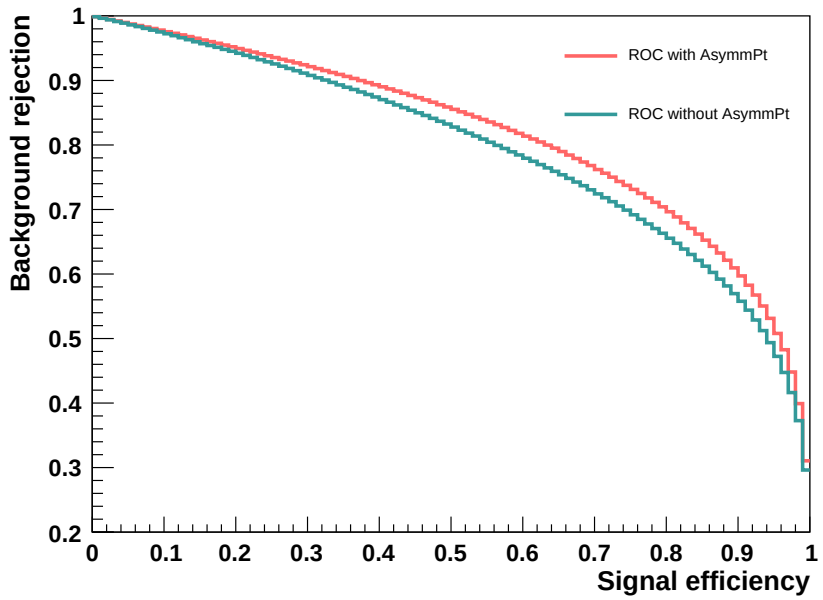

Figure 4.5: ROC curves, the area under the curve for the green one is 0.797, for the red one is 0.819.

4.4.3 Cut efficiencies

To calculate the probability of a Λ_c^+ being produced in high energy pp collisions, it is necessary to measure how many of these particles appear in our data. This measurement is made particularly challenging due to the high combinatorial background, specifically at low transverse momenta. So the first step in estimating the particles number is apply a cut on the output response, that allows to eliminate a relevant part of the background without possibly lose too many signal events. TMVA supplies a graph (figure 4.6) that display signal and background efficiencies, obtained from cutting on the classifier outputs, versus the cut value. The graph also shows the signal purity, the product of signal efficiency and purity, which correspond to the expected number of signal and background events before cutting and the significance. Also the optimal cuts according to the best significance are shown.
To compare the two classifiers it was applied a cut to maintain the same efficiency of 90%.

The cut on the output for the first model without `AsymmPt` is 0.071 and for the second with `AsymmPt` is 0.074. Of course, the efficiency is calculated on the testing data set, whose output is known, so it is only an esteem for the experimental data on which the algorithm is applied. Additionally, TMVA provides an accurate cut value that maximizes the significance and the analyses was done also with these cut values, corresponding to 0.0992 (without `AsymmPt`) and 0.1181 (with `AsymmPt`).

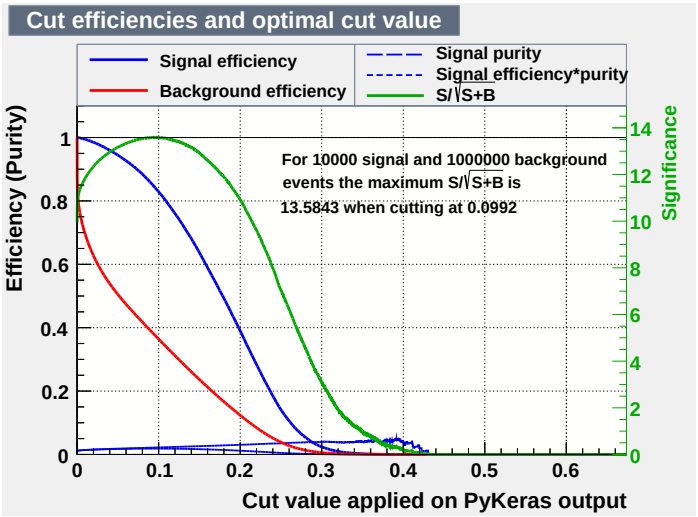

(a)

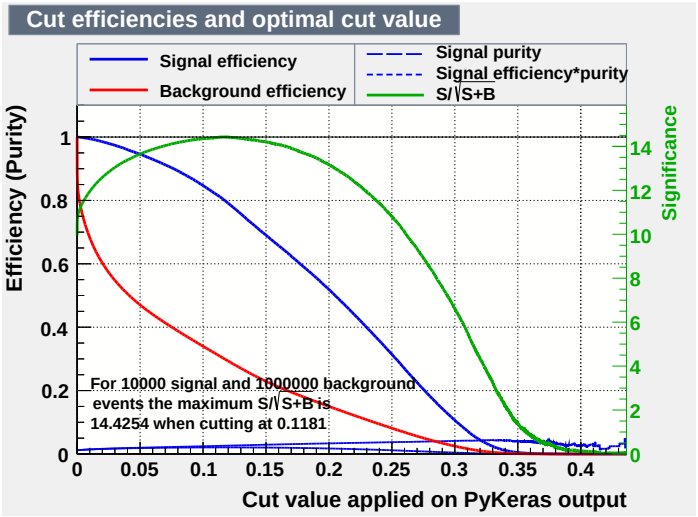

(b)

Figure 4.6: Classifier cut efficiencies estimated for 10000 signal events and 1000000 background events, (a) without `AsymmPt`, (b) with `AsymmPt`.

4.5 Application and analysis

After the two versions of the algorithm were trained and tested, they were applied to real data of pp collisions at center of mass energy of 13 TeV. The events processed during this phase were of the order of 30 millions, and the algorithm took several hours to run through all of them. The application macro created two histograms: a one-dimensional histogram representing the distribution of the PyKeras responses, and a two-dimensional histogram that allows to analyze how the output is correlated to the invariant mass. Ideally, in the region of the correct mass of Λ_c^+ the model should have assigned a score closer to 1. By projecting the two-dimensional histogram it was possible to recover the mass invariant histogram, ready to be fitted.
The background was modelled with a third degree polynomial function and the fit background function was subtracted from the histogram. The obtained shape, representing the signal, was fitted with a gaussian, whose width σ is mainly due to the track resolution of ALICE detectors and for this reason fixed at the expected value from the simulation ($\sigma = 0.076\,\mathrm{MeV/c^2}$). The results with the cut on the classifier response made to maintain the efficiency at 90% are visible in figure 4.7. The Λ_c^+ mass, the yield, that is the actual number of Λ_c^+ calculated through the integral of the histogram and the significance for both methods are summarized in table 4.1. The classifier that has been trained adding

	Mass of Λ_c^+ ($\mathrm{MeV/c^2}$)	Yield	Significance
Without `AsymmPt`	2.2890 ± 0.0010	9645 ± 1009	7.68
With `AsymmPt`	2.2888 ± 0.0009	9808 ± 962	8.18

Table 4.1: Main fitting results of the analysis conducted with a cut of the output of the classifier that set the efficiency at 90%.

the variable `AsymmPt` performed better and gave a slightly more precise result, as can be seen by comparing the signal-to-noise (S/B) ratio (0.0069 with and 0.0062 without the `AsymmPt` variable) and the significance (8.18 and 7.68). Furthermore, even with regard to statistical uncertainty, the analysis with the `AsymmPt` variable seems slightly better (10% versus 11%). However, the results appear to be quite similar, like the ROC curves suggested (figure 4.5), with little difference between the two classifier.

An analogous analysis was performed with the only change being the cut value of the classifier response. TMVA accurately calculates the optimal cut value that maximize the significance, as shown in figure 4.6. These values were adopted in this version, with 0.0992 for the classifier trained without `AsymmPt`, and 0.1181 for the other one. In this case, the signal efficiencies on the training set were 0.8313 (without `AsymmPt`) and 0.7917 (with `AsymmPt`). Table 4.2 compares quantitatively the outcomes, and the fit results are displayed in figure 4.8.

	Mass of Λ_c^+ (MeV/c^2)	Yield	Significance
Without `AsymmPt`	2.2888 ± 0.0009	9600 ± 917	8.28
With `AsymmPt`	2.2886 ± 0.0009	8756 ± 825	8.48

Table 4.2: Main fitting results of the analysis conducted with a cut of the output of the classifier that maximized the significance.

Both versions lead overall to similar outcomes, with the main difference being the yield in the second analysis version with `AsymmPt`, that is 8756 ± 825 (see table 4.2). Although this is the lowest yield obtained, it is not unexpected since the cut value was the highest compared to the other ones, and the value is compatible with the rest within the uncertainty. However, even if only slightly, the performance provided by the algorithm with the `AsymmPt` variable is better in this case too, with an S/B ratio of 0.0084 against 0.0074 (+14%) and a significance of 8.48 against 8.28 (+2.4%).

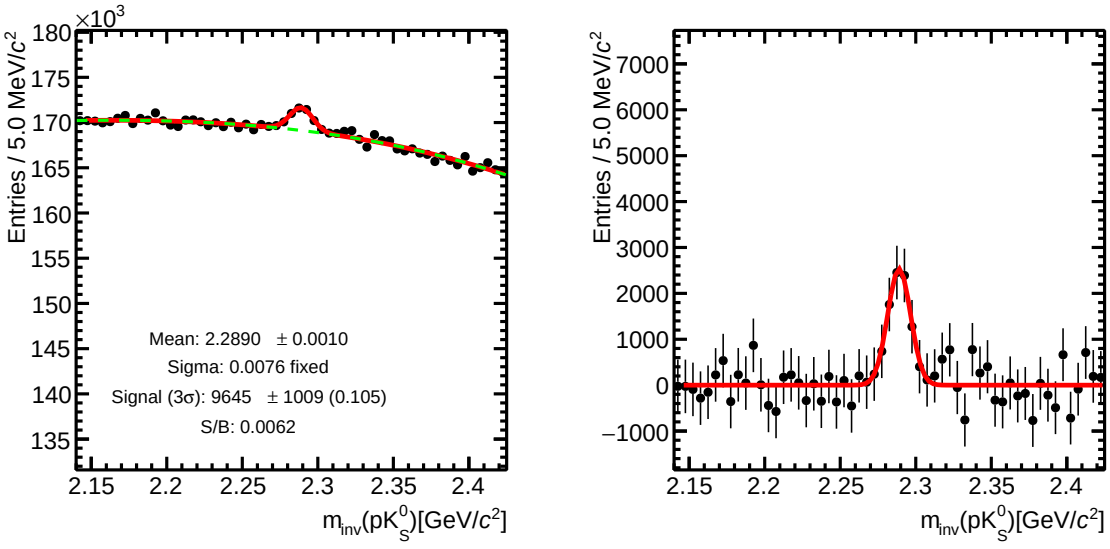

(a)

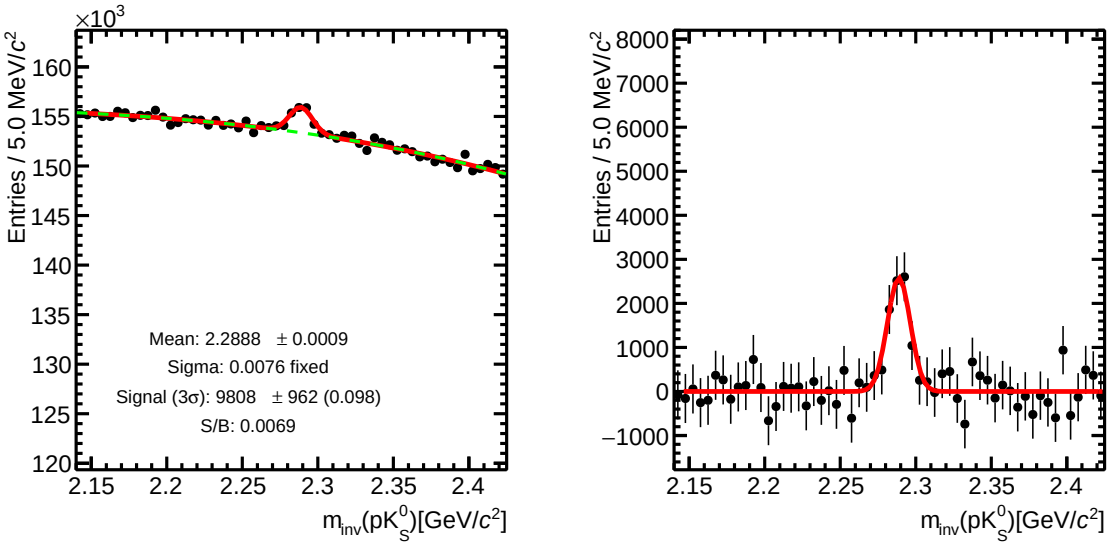

(b)

Figure 4.7: Mass invariant histogram with the background fitted with a third degree polynomial function on the left, on the right there is the mass invariant histogram with the background subtracted and fitted with a gaussian. The figure (a) represents the fit results without using `AsymmPt`, in figure (b) it is depicted the outcome of the analysis made with the variable `AsymmPt`. A cut value that set the efficiency of 90% was applied to the labeling algorithm.

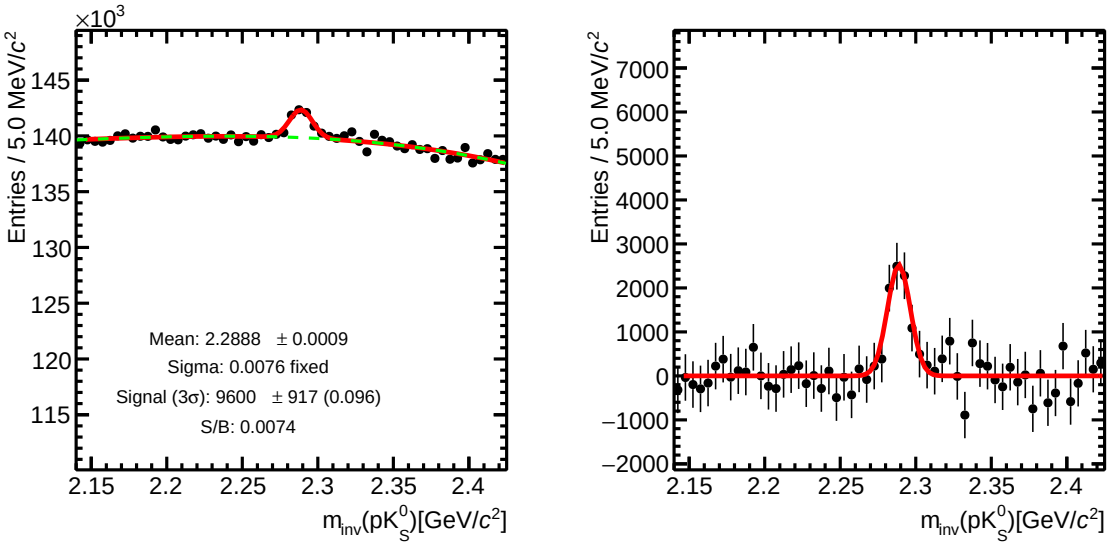

(a)

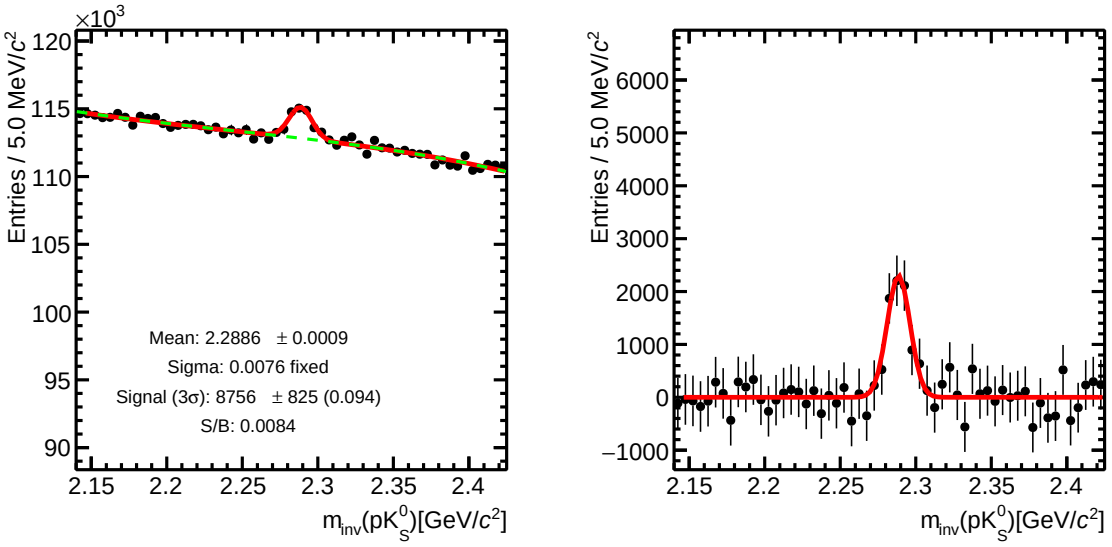

(b)

Figure 4.8: Mass invariant histogram with the classifier output cut that maximize the significance. The background fitted with a third degree polynomial function is on the left, on the right there is the mass invariant histogram with the background subtracted and fitted with a gaussian. The figure (a) represents the fit results without using `AsymmPt`, in figure (b) it is depicted the outcome of the analysis made with the variable `AsymmPt`.

Conclusions

Recent measurements made at ALICE in proton-proton collisions revealed that there is a significantly larger fraction of charm quarks hadronising to baryons, compared to e^+e^- and ep collisions. This challenges the assumption that fragmentation functions are universal and can therefore be deduced from e^+e^- results. To correctly interpret the data, other hadronisation mechanisms beyond the fragmentation process need to be considered and theoretical hypothesis have been proposed, each of them relying on different assumptions. These models are able to reproduce in general the data, but differ at low transverse momenta, therefore especially at low p_T obtaining precise values of baryon production is essential to understand which model aligns best with ALICE outcomes.

In this present work, the Λ_c^+ signal was reconstructed via the decay channel $\Lambda_c^+ \rightarrow pK_s^0$ in the transverse momentum region of $1 < p_T < 2\,\mathrm{GeV/c}$ in pp collisions at $\sqrt{s} = 13\,\mathrm{TeV}$ using a neural network model in TMVA. The employment of machine learning was necessary due to the low signal-to-background ratio and the short lifetime of Λ_c^+. The machine learning algorithm was trained twice: with and without an additional variable that presented itself as a potentially privileged candidate for training the algorithm, because of the different distribution for the signal and background in the training phase. Both versions were applied to real, experimental data to test their effectiveness. A cut was applied on the classifier response to chop out a good portion of the background, and the analysis was performed firstly by balancing efficiency and then by optimizing the significance with the appropriate cuts. The background was modelled with a third degree polynomial and the mass invariant signal was fitted with a gaussian. Finally, the yield was extracted with the integral of the gaussian and in all versions, the extracted yields were found to be compatible with each other within the uncertainties. The analysis performed with the additional variable was slightly better, showing improved values for the signal-to-background ratio, statistical significance, and statistical uncertainty; however, the improvement is not sufficient to significantly enhance the current precision of the extracted signal, which is not capable of favoring any specific model. Future work aims to improve precision and hopefully contribute to the understanding of charm-baryon production in small system at LHC.

Besides that, the discovery of enhanced baryon production in pp collision, as well as other similarities observed in Pb–Pb collisions, raises questions about the conventional view that QGP is only formed in heavy-ions collisions. Therefore, further experimental and theoretical efforts are needed to fully understand the charm quark hadronisation mechanisms and the underlying dynamics in hadronic collisions at the LHC. Future work, maybe with the upgraded ALICE experiments (ALICE 2 and ALICE 3) will be crucial in addressing these questions.

Acknowledgements

Il primo ringraziamento va obbligatoriamente al prof. Andrea Alici, per la sua costante presenza e supporto durante tutto il lavoro di tesi e per essere una delle persone più disponibili incontrate in tutto il mondo accademico, sono molto felice di aver concluso questo percorso così.
Passando al lato personale, penso che siamo la somma delle persone che più ci stanno vicino, quindi questo spazio è dedicato a chi fa parte di me. Innanzitutto, ringrazio la mia famiglia per avermi supportato al meglio ed essersi sempre fidata: grazie babbo per non aver mai dimenticato di augurarmi "in bocca al lupo", grazie mamma perché non c'è un momento in cui non ti senta accanto a me e infine grazie Andrea per avermi fatto capire che ingegneria proprio non faceva per me.
Grazie a chi mi ha fatto e continua a farmi sentire a casa: la convivenza con te, Anna, continua ad essere una delle mie cose preferite della mia vita bolognese. Alla Vero, come dicesti tu "per me sei tipo famiglia", non saprei descrivere in modo migliore il nostro rapporto. Grazie ai miei compagni di studio preferiti: alla Mari, che ha sempre i cassoni pronti per le nostre sessioni di studio, e a Franci: in questi anni non hai mai perso occasione di farmi ridere, grazie di tirare sempre fuori la parte più stupida di me, mi manchi ogni volta che sono in biblioteca e tu non ci sei. Grazie a Fabio, quello bravo con le parole sei tu, ma ti sono grata per le nostre chiacchierate, non vedo l'ora di farne altre mille, anche se so che dovrò essere io ad organizzare, perché tu altrimenti perderesti qualcosa per strada. A Gio, alla nostra amicizia, al tuo entusiasmo e genuinità, alla granita e ai nostri momenti insieme, cosa è meglio di così? Cami, so che non ti piacciono queste cose, mi limiterò quindi a ribadire che sei ciò che di più bello Bologna mi ha dato. Grazie ai miei compagni di Erasmus, mi avete insegnato che "non siamo uguali e non lo saremo mai, e questa è la cosa più simile a tutti che abbiamo".
Grazie ai miei amici toscani. Siete tanti per nominarvi tutti, ma ci tengo a dirvi che sono cresciuta con e attraverso di voi e per questo motivo vi porto con me in ogni esperienza che faccio. Grazie per darmi sempre leggerezza, spontaneità e immenso affetto, vi voglio bene.
Infine, grazie a Piazza Grande e a Bologna, che è più di una splendida città, ma un mosaico di posti, libri, musica, serate e persone, una parte di me resterà sempre qui.

Bibliography

[1] *The Higgs Boson*. https://home.cern/science/physics/higgs-boson. Accessed: 2024-09-29.

[2] *The Standard Model*. https://home.cern/science/physics/standard-model. Accessed: 2024-09-29.

[3] Tiantian Cheng. "Measurements of charm-strange baryon production with ALICE at the LHC". Other thesis. CCNU, Wuhan, Inst. Part. Phys., Mar. 2024.

[4] Particle Data Group et al. "Review of Particle Physics". In: *Progress of Theoretical and Experimental Physics* 2020.8 (Aug. 2020), p. 083C01. ISSN: 2050-3911. DOI: 10.1093/ptep/ptaa104. eprint: https://academic.oup.com/ptep/article-pdf/2020/8/083C01/34673739/rpp2020-vol2-1823-2014_17.pdf. URL: https://doi.org/10.1093/ptep/ptaa104.

[5] S. Braibant, G. Giacomelli, and M. Spurio. *Particles and Fundamental Interactions: An Introduction to Particle Physics*. Undergraduate Lecture Notes in Physics. Springer Netherlands, 2011. ISBN: 9789400724631. URL: https://books.google.it/books?id=0Pp-f0G9_9sC.

[6] D. Griffiths. *Introduction to Elementary Particles*. New York, USA: John Wiley & Sons, 1987.

[7] *Heavy ions and quark-gluon plasma*. https://home.cern/science/physics/heavy-ions-and-quark-gluon-plasma. Accessed: 2024-09-28.

[8] Gergely Endrődi. "QCD phase diagram: overview of recent lattice results". In: *Journal of Physics: Conference Series* 503.1 (Apr. 2014), p. 012009. DOI: 10.1088/1742-6596/503/1/012009. URL: https://dx.doi.org/10.1088/1742-6596/503/1/012009.

[9] Jiaxing Zhao et al. "Heavy-flavor hadron production in relativistic heavy ion collisions at energies available at BNL RHIC and at the CERN LHC in the EPOS4HQ framework". In: *Phys. Rev. C* 110 (2 Aug. 2024), p. 024909. DOI: 10.1103/PhysRevC.110.024909. URL: https://link.aps.org/doi/10.1103/PhysRevC.110.024909.

[10] Min He, Hendrik van Hees, and Ralf Rapp. "Heavy-quark diffusion in the quark–gluon plasma". In: *Progress in Particle and Nuclear Physics* 130 (2023), p. 104020. ISSN: 0146-6410. DOI: https://doi.org/10.1016/j.ppnp.2023.104020. URL: https://www.sciencedirect.com/science/article/pii/S0146641023000017.

[11] ALICE Collaboration. *The ALICE experiment – A journey through QCD*. 2022. arXiv: 2211.04384 [nucl-ex]. URL: https://arxiv.org/abs/2211.04384.

[12] Shreyasi Acharya et al. "Charm production and fragmentation fractions at midrapidity in pp collisions at $\sqrt{s}$ = 13 TeV". In: *JHEP* 12 (2023), p. 086. DOI: 10.1007/JHEP12(2023)086. arXiv: 2308.04877.

[13] S. Acharya et al. "First measurement of Λ_c^+ production down to $p_T = 0$ in pp and in p-Pb collisions at $\sqrt{S_{NN}} = 5.02$ TeV". In: *Physical Review C* 107.6 (June 2023). ISSN: 2469-9993. DOI: 10.1103/physrevc.107.064901. URL: http://dx.doi.org/10.1103/PhysRevC.107.064901.

[14] *First lead-ion collisions in the LHC at record energy*. https://alice-collaboration.web.cern.ch/Nov2022_leadtest. Accessed: 2024-10-01.

[15] "The ALICE experiment at the CERN LHC". In: *Journal of Instrumentation* 3.08 (Aug. 2008), S08002. DOI: 10.1088/1748-0221/3/08/S08002. URL: https://dx.doi.org/10.1088/1748-0221/3/08/S08002.

[16] *ALICE Collaboration: ALICE*. https://alice-collaboration.web.cern.ch/. Accessed: 2024-10-03.

[17] ALICE collaboration. "Alignment of the ALICE Inner Tracking System with cosmic-ray tracks". In: *Journal of Instrumentation* 5.03 (Mar. 2010), P03003. DOI: 10.1088/1748-0221/5/03/P03003. URL: https://dx.doi.org/10.1088/1748-0221/5/03/P03003.

[18] J. Alme et al. "The ALICE TPC, a large 3-dimensional tracking device with fast readout for ultra-high multiplicity events". In: *Nuclear Instruments and Methods in Physics Research Section A: Accelerators, Spectrometers, Detectors and Associated Equipment* 622.1 (Oct. 2010), pp. 316–367. ISSN: 0168-9002. DOI: 10.1016/j.nima.2010.04.042. URL: http://dx.doi.org/10.1016/j.nima.2010.04.042.

[19] A. Alici. "The MRPC-based ALICE time-of-flight detector: Status andperformance". In: *Nuclear Instruments and Methods in Physics Research Section A: Accelerators, Spectrometers, Detectors and Associated Equipment* 706 (Apr. 2013), pp. 29–32. ISSN: 0168-9002. DOI: 10.1016/j.nima.2012.05.004. URL: http://dx.doi.org/10.1016/j.nima.2012.05.004.

[20] Yann Coadou. "Boosted Decision Trees". In: *Artificial Intelligence for High Energy Physics*. WORLD SCIENTIFIC, 2022. ISBN: 9789811234033. DOI: 10.1142/9789811234033_0002. URL: http://dx.doi.org/10.1142/9789811234033_0002.

[21] Michael A. Nielsen. *Neural Networks and Deep Learning*. 2018. URL: http://neuralnetworksanddeeplearning.com/.

[22] Martín Abadi et al. *TensorFlow: Large-Scale Machine Learning on Heterogeneous Systems*. Software available from tensorflow.org. 2015. URL: https://www.tensorflow.org/.

[23] François Chollet et al. *Keras*. https://keras.io. 2015.

[24] Andreas Hocker et al. "TMVA - Toolkit for Multivariate Data Analysis". In: (Mar. 2007). arXiv: physics/0703039.

[25] Torbjörn Sjöstrand et al. "An introduction to PYTHIA 8.2". In: *Computer Physics Communications* 191 (2015), pp. 159–177. ISSN: 0010-4655. DOI: https://doi.org/10.1016/j.cpc.2015.01.024. URL: https://www.sciencedirect.com/science/article/pii/S0010465515000442.

[26] R Brun et al. *GEANT 3: user's guide Geant 3.10, Geant 3.11; version*. Geneva: CERN, 1987. URL: https://cds.cern.ch/record/1119728.

[27] M. Tanabashi et al. "Review of Particle Physics". In: *Phys. Rev. D* 98 (3), p. 030001. DOI: 10.1103/PhysRevD.98.030001. URL: https://link.aps.org/doi/10.1103/PhysRevD.98.030001.